A TWO-DIMENSIONAL FINITE ELEMENT ADVECTION MODEL WITH VARIABLE RESOLUTION

Mark Elwood Older

NAVAL POSTGRADUATE SCHOOL
Monterey, California

THESIS

A TWO-DIMENSIONAL FINITE ELEMENT ADVECTION MODEL WITH VARIABLE RESOLUTION

by

Mark Elwood Older III

June 1981

Thesis Advisor: R. T. Williams

Approved for public release; distribution unlimited.

SECURITY CLASSIFICATION OF THIS PAGE (When Data Entered)

REPORT DOCUMENTATION PAGE		READ INSTRUCTIONS BEFORE COMPLETING FORM
1. REPORT NUMBER	2. GOVT ACCESSION NO.	3. RECIPIENT'S CATALOG NUMBER
4. TITLE (and Subtitle) A Two-Dimensional Finite Element Advection Model with Variable Resolution		5. TYPE OF REPORT & PERIOD COVERED Master's Thesis; June 1981
		6. PERFORMING ORG. REPORT NUMBER
7. AUTHOR(s) Mark Elwood Older III		8. CONTRACT OR GRANT NUMBER(s)
9. PERFORMING ORGANIZATION NAME AND ADDRESS Naval Postgraduate School Monterey, California 93940		10. PROGRAM ELEMENT, PROJECT, TASK AREA & WORK UNIT NUMBERS
11. CONTROLLING OFFICE NAME AND ADDRESS Naval Postgraduate School Monterey, California 93940		12. REPORT DATE June 1981
		13. NUMBER OF PAGES 84
14. MONITORING AGENCY NAME & ADDRESS(if different from Controlling Office)		15. SECURITY CLASS. (of this report) Unclassified
		15a. DECLASSIFICATION/DOWNGRADING SCHEDULE

16. DISTRIBUTION STATEMENT (of this Report)

Approved for public release; distribution unlimited.

17. DISTRIBUTION STATEMENT (of the abstract entered in Block 20, if different from Report)

18. SUPPLEMENTARY NOTES

19. KEY WORDS (Continue on reverse side if necessary and identify by block number)

Finite Element Method
Galerkin Method
Variable Resolution

20. ABSTRACT (Continue on reverse side if necessary and identify by block number)

Many meteorological forecast applications require the use of grids that have a high resolution in a particular area of interest, while allowing coarser resolution elsewhere. Conventional finite difference models often use nested grids to this end. In recent years, finite element models have been offered as an alternative. In this study, the two-dimensional advection equation with diffusion is defined over a rectangular domain. The Galerkin technique is applied to linear basis

DD FORM 1 JAN 73 1473 EDITION OF 1 NOV 65 IS OBSOLETE
S/N 0102-014-6601 |
(Page 1)

SECURITY CLASSIFICATION OF THIS PAGE (When Data Entered)

functions on triangular elements. The model is tested to determine the sensitivity of the forecast to various nodal geometries. Both equilateral and right triangular elements are tested. It is found that the equilateral arrangement consistently yields a superior forecast. Other tests are conducted in which the resolution is varied smoothly versus abruptly over the domain. The smoothly varying case gives results that are dramatically improved over the abruptly varying case. Among the conclusions is the fact that, for a given maximum resolution, the more slowly and smoothly the element size is changed, the better the forecast obtained.

Approved for public release, distribution unlimited

A Two-Dimensional Finite Element Advection Model with Variable Resolution

by

Mark Elwood Older III
Captain, United States Air Force
B.S., University of Michigan, 1972

Submitted in partial fulfillment of the
requirements for the degree of

MASTER OF SCIENCE IN METEOROLOGY

from the

NAVAL POSTGRADUATE SCHOOL
June 1981

ABSTRACT

Many meteorological forecast applications require the use of grids that have a high resolution in a particular area of interest, while allowing coarser resolution elsewhere. Conventional finite difference models often use nested grids to this end. In recent years, finite element models have been offered as an alternative. In this study, the two-dimensional advection equation with diffusion is defined over a rectangular domain. The Galerkin technique is applied to linear basis functions on triangular elements. The model is tested to determine the sensitivity of the forecast to various nodal geometries. Both equilateral and right triangular elements are tested. It is found that the equilateral arrangement consistently yields a superior forecast. Other tests are conducted in which the resolution is varied smoothly versus abruptly over the domain. The smoothly varying case gives results that are dramatically improved over the abruptly varying case. Among the conclusions is the fact that, for a given maximum resolution, the more slowly and smoothly the element size is changed, the better the forecast obtained.

TABLE OF CONTENTS

LIST OF TABLES

LIST OF FIGURES

ACKNOWLEDGEMENTS

The author wishes to thank Lt. R. G. Kelly whose research was the precursor to this investigation. The algorithm and some of the computer code were borrowed from that research. Particular thanks are extended to Dr. M. J. P. Cullen whose personal suggestions provided the direction for this work. Professors R. L. Haney and R. T. Williams reviewed the manuscript and made many useful comments on it. The manuscript was carefully typed by Ms. M. Marks.

The author wishes to give special thanks to his wife, Michele, without whose patient assistance and support this work would not have been possible.

I. INTRODUCTION

Sub-Synoptic scale meteorological elements are usually not represented or forecast well by coarse mesh numerical models. This situation may be improved by increasing the resolution of the grid. However, a uniform reduction of the grid mesh requires a significant increase in computational time and computer storage. Hence this is a limitation on the practical resolution, and therefore accuracy, for a uniform grid. The conventional solution is to nest grids so that the geographical area or meteorological feature of interest is covered by a fine mesh, and less interesting areas or features are left with a coarse mesh. The advantage of this technique is to increase accuracy in the desired area while keeping the computational storage and time requirements within reasonable limits. There are, however, two disadvantages to nested grids. First, the abrupt change in grid size at the boundaries of the fine mesh generates noise in the solution. Second, boundary conditions for the fine mesh must be interpolated from the coarse mesh.

A better technique would allow the grid to vary smoothly and continuously over the domain rather than in abrupt jumps. However, such a highly variable grid greatly complicates a finite difference numerical model. As an alternative to such a finite difference technique, consider the Finite Element Method (FEM). This method has long been used in mechanical engineering but has been adapted to meteorology only during

the last decade. Pioneering work in meteorological applications was done by Cullen (1973). Staniforth and Mitchell (1978) and Staniforth and Daley (1977) have devised more recent forecast models. The most recent FEM meteorological model at the Naval Postgraduate School was written by Kelly and Williams (1976) and is the precursor to this study.

The great attractions of the FEM are the more accurate phase speeds [Haltiner and Williams (1980)], and its suitability to non-uniform grids. The method involves the division of the domain into a number of elements and then defining an equation for each node of each element. Thus, solution requires solving a large number of linear equations simultaneously. However, there is no limitation on the size of the elements or the shape of the domain. The method is easily adapted to concentration of small elements in areas of interest and assignment of larger elements to other areas.

The purpose of this investigation is to determine the sensitivity of a FEM model to different grid geometries. The model used is a two-dimensional advection model with diffusion. It was deliberately chosen because of its simplicity. By keeping the model simple, all variations in the results can be attributed to differences in geometric and initial conditions rather than inaccuracies in the equation formulation. In addition to sensitivity studies, the model can be adapted as an operational predictor of any scalar field such as cloudiness, vorticity, temperature or precipitation.

The Galerkin technique is employed to transform the differential equation for the dependent variable into a set of algebraic equations. Triangular elements are used with the area coordinate system. Later chapters will show that these techniques greatly simplify the computations.

II. THE METHOD

The Galerkin technique will be explained by first an example, after Crandall (1956), and then the application to the FEM, after Kelly and Williams (1976).

A. EXAMPLE

Consider a simple differential equation, that which governs the cooling of an object

$$\begin{aligned} x &= 1 \qquad && t = 0 \\ \frac{dx}{dt} &= -x \qquad && t > 0 \end{aligned} \tag{II-1}$$

with the solution defined on the interval $0 < t < 1$.

The critical step is to select a trial family of approximate solutions. (The members of a trial family are often called basis functions.) For simplicity, consider the second order trial-solutions

$$\hat{x} = 1 + c_1 t + c_2 t^2 \tag{II-2}$$

where $\hat{x}$ is the approximate solution.

The object is now to determine the coefficients c_1 and c_2. Next, form the residual, R(t) from II-1

$$R = \frac{dx}{dt} + x \tag{II-3}$$

substituting II-2 into II-3

$$R = 1 + c_1(1 + t) + c_2 (2t + t^2) \qquad \text{II-4}$$

Now we want to adjust c_1 and c_2 so that II-4 stays close to zero on the interval $0 < t < 1$.

The above discussion applies to any weighted residual technique; however, Galerkin's technique has two requirements:

1. The *weighted averages* of the residual must vanish over the interval.
2. The *weighting functions* must be the same functions of t as were used to construct the trial family (in II-2). In this case those weighting functions are t and t^2.

That is, the weighted averages are formed by multiplying the residual by the weighting functions, integrating the product over the interval and setting the result equal to zero.

$$\int_0^1 t\, R\, dt = 0$$

and $$\qquad \text{II-5}$$

$$\int_0^1 t^2 R\, dt = 0$$

Substituting II-4 into II-5

$$\int_0^1 t\,R\,dt = \int_0^1 [t + c_1(t+t^2) + c_2(2t^2+t^3)]dt$$

$$= \frac{1}{2} + \frac{5}{6}c_1 + \frac{11}{12}c_2 = 0 \qquad \text{II-6a}$$

and

$$\int_0^1 t^2 R\,dt = \int_0^1 [t^2 + c_1(t^2+t^3) + c_2(2t^3+t^4)]dt$$

$$= \frac{1}{3} + \frac{7}{12}c_1 + \frac{7}{10}c_2 = 0 \qquad \text{II-6b}$$

Solving II-6a and b for c_1 and c_2 we find:

$$c_1 = -.9143,\ c_2 = 0.2857$$

So that the approximate solution is

$$\hat{x} = 1 - 0.9143\,t + 0.2857\,t^2$$

The exact solution to Equation II-1 is

$$x = e^{-t}$$

Figure 1 shows the plots of the exact solution and the approximate solution. Note that this technique yields the best fit only on the desired interval $0 < t < 1$ and that the solutions may diverge from the interval.

In general, Galerkin's technique will reduce a partial differential equation to a family of N algebraic equations, where N is the number of basis functions. In this example Galerkin's technique has reduced II-1 to two equations, II-6a and II-6b, in the two basis functions t and t^2.

B. APPLICATION TO THE FEM

The Finite Element Method divides the domain into discrete segments called elements with points (called nodes) arranged about the perimeter of the elements. The basis functions are then defined locally. These basis functions are usually low order polynomials that must be piece-wise continuous. A one-dimensional example is Figure 2 wherein the domain (x-axis) is divided into four elements (line segments) W through Z. All of the basis functions (A-C) are linear rising to a value of unity over each node (points 2 through 4) and are zero elsewhere. Now, if a variable S is defined over node 3, for example, then it may be approximated by

$$S = \gamma_2 V_A + \gamma_3 V_B + \gamma_4 V_C \qquad \text{II-7}$$

where γ_2, γ_3 and γ_4 are the values of S at nodes 2, 3 and 4 respectively and V_A, V_B, V_C are the basis functions A, B, and C respectively.

Equation II-7 may be substituted into any equation in which S appears. An equation using II-7 can be written for each node, by multiplying the basic equation by the basis function and integrating over the domain.

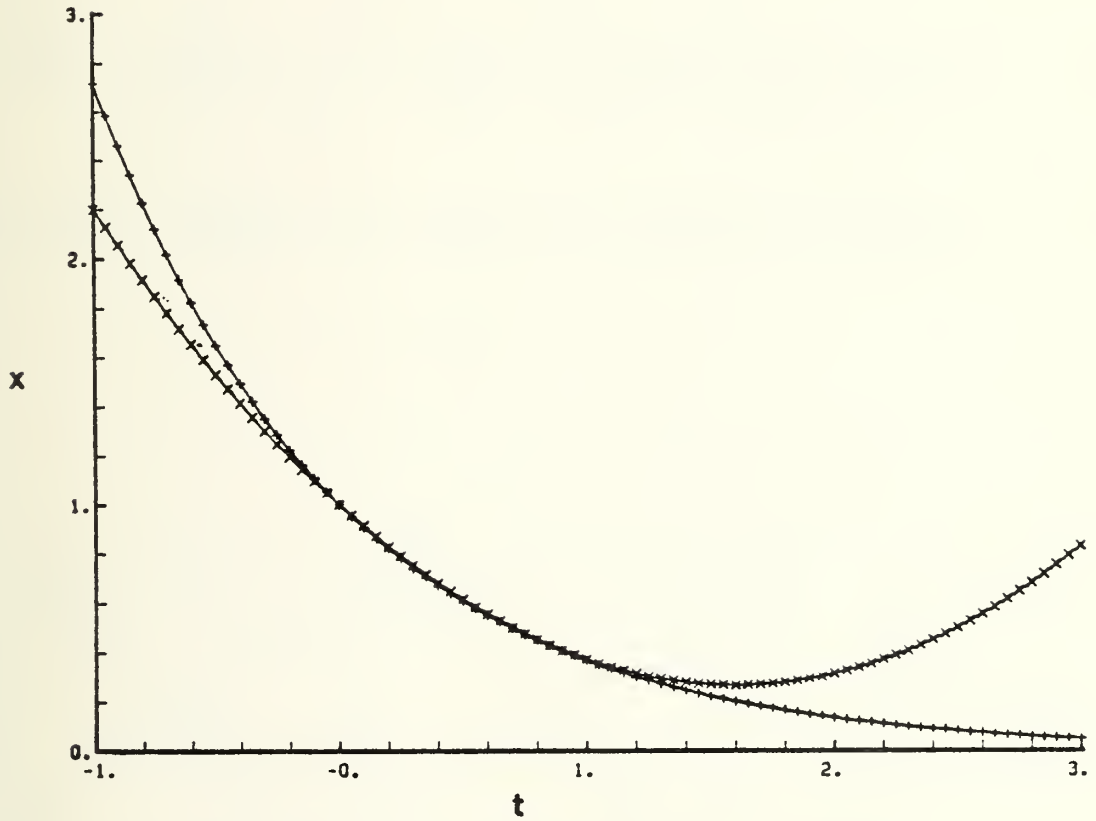

Figure 1. Solutions to cooling object example. Approximate solution is the curve connecting the 'x' signs. Exact solution is the curve connecting the '+' signs.

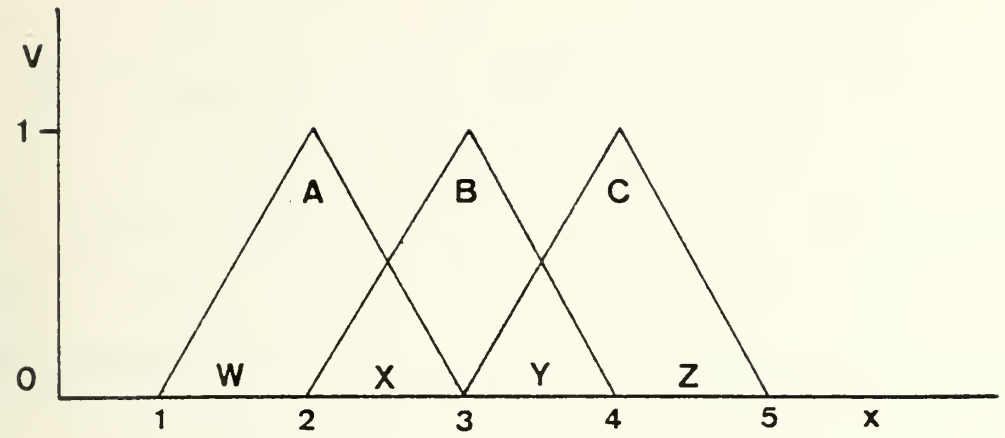

Figure 2. One-dimensional example of linear basis functions.

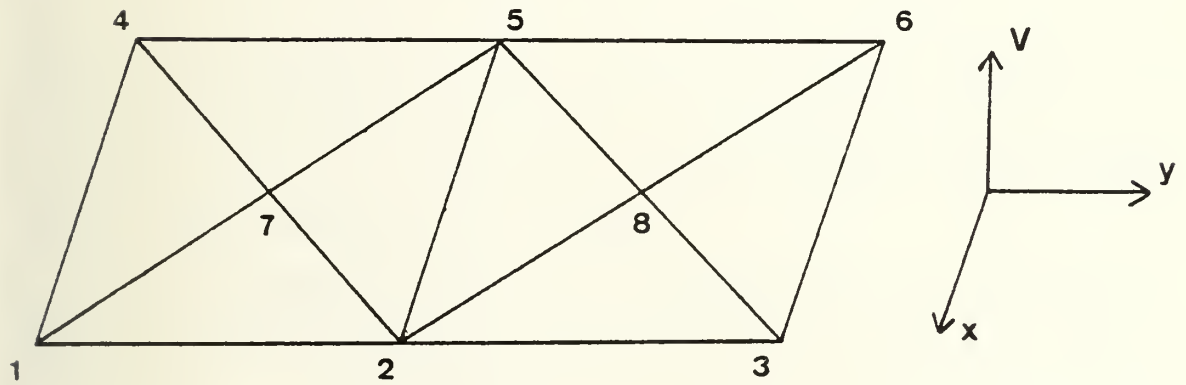

Figure 3. A domain with eight nodes and eight triangular elements.

The end result is a system of N equations in N unknowns, where N is the number of nodes. Fortunately, in matrix form, these equations are often tridiagonal and may be solved with great economy.

In two dimensions the basis functions are somewhat different, but the mathematics is identical. In Figure 3, the domain has been divided into eight triangular elements with eight nodes. Figure 4 shows the basis function (outlined in heavy black) at node 7 that must span all the elements about node 7. Note that the function has value of unity at node 7 and decreases linearly to zero at all surrounding nodes. Figure 5 shows another basis function, but this one at node 5. Each node has a similar basis function about it.

The value of a variable S may be approximated at any node i by

$$S = \sum_{j} \gamma_j \quad V_j \qquad \text{II-8}$$

where j ranges over all the nodes connected to node i including i itself, γ_j is the value of S at node j and V_j is the value, at the j-th node, of the basis function of the i-th node.

As in the one-dimensional case, an equation like II-8 is written for each node, i, then multiplied by the basis function and integrated over the domain. The resultant equation set, in matrix form, contains an n by n square matrix where n is the number of nodes. Although this matrix is usually not tridiagonal, careful selection of a nodal numbering system would yield a matrix that is strongly banded and fairly easily solvable. Alternatively, with these sparse matricies, iterative methods converge rapidly.

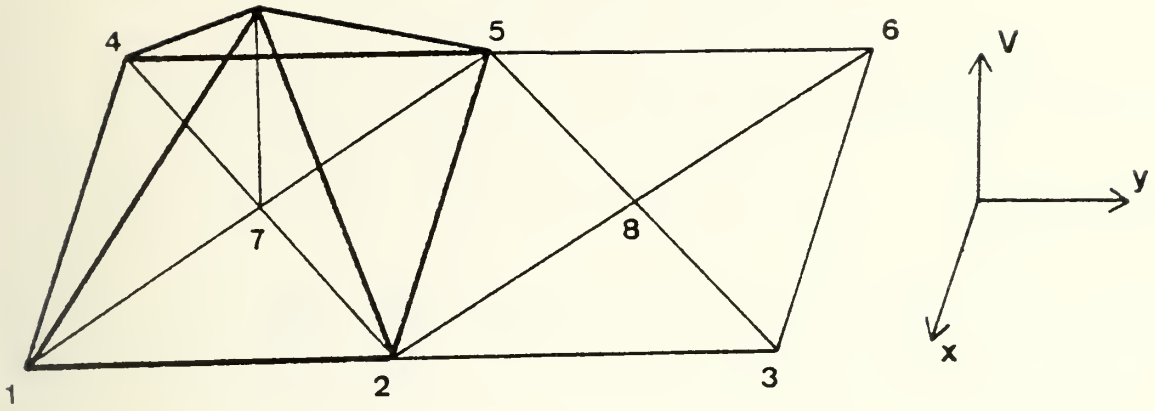

Figure 4. The linear basis function associated with node seven.

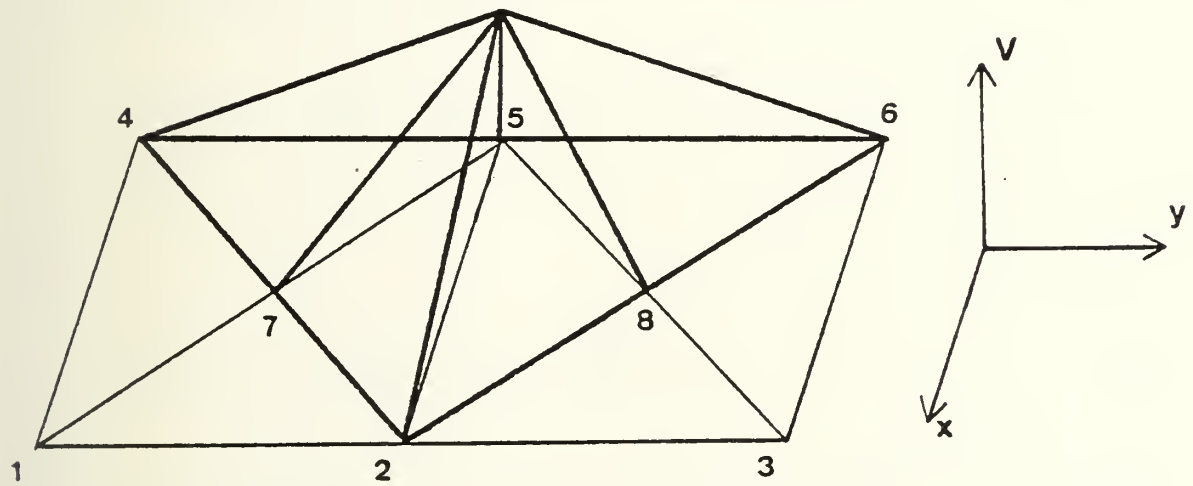

Figure 5. Another linear basis function on the same domain.

III. EQUATION FORMULATION

The equation of interest to the investigation is the two-dimensional advection equation with second order diffusion:

$$\frac{\partial S}{\partial t} + u \frac{\partial S}{\partial x} + v \frac{\partial S}{\partial y} - K_h \nabla^2 S = 0 \qquad \text{III-1}$$

Define an inner product of two functions f(x,y) and g(x,y) as

$$\int_y \int_x fg \, dx \, dy \equiv \langle f,g \rangle$$

Following the Galerkin technique, form the residue and find the weighted averages, using the basis functions as weighting functions. Neglect the diffusion term at this stage.

$$\int_y \int_x [\frac{\partial S}{\partial t} + u \frac{\partial S}{\partial x} + v \frac{\partial S}{\partial y}] \, V \, dx \, dy = 0$$

or

$$\langle \frac{\partial S}{\partial t} , V \rangle + \langle u \frac{\partial S}{\partial x} , V \rangle + \langle v \frac{\partial S}{\partial y} , V \rangle = 0 \qquad \text{III-2}$$

where V is the weighting function. Although the domain of integration is over the entire range of x and y, it will soon be shown that V is zero everywhere except locally around a specific node. So that for any node, III-2 is non-zero only when within one grid increment of that node.

The variables will have the form

$$S = \gamma_j V_j$$

$$u = \alpha_j V_j \qquad \text{III-3}$$

$$v = \beta_j V_j$$

where the repeated subscripts indicate summation over the range of the subscript. The coefficient is a function of time only and the basis function is a function of space only. That is

$$S = \gamma_j V_j = \sum_j \gamma_j(t) V_j(x,y)$$

etc.

The critical step is the requirement that the weighting function in III-2 be the same as the basis function in III-3. Substitution of III-3 into III-2 yields

$$\langle \dot{\gamma}_j V_j, V_i \rangle + \langle \alpha_k V_k \gamma_j \frac{\partial V_j}{\partial x}, V_i \rangle$$

$$+ \langle \beta_k V_k \gamma_j \frac{\partial V_j}{\partial y}, V_i \rangle = 0 \qquad \text{III-4}$$

where the dot indicates a time derivative.

Applying first the Galerkin technique and then the Gauss Divergence Theorem to the diffusion term yields

$$\int_y \int_x K_h(\nabla^2 S)V_i \, dxdy = K_h \int_y \int_x \nabla \cdot (\nabla S)V_i \, dxdy$$

$$= K_h \int_y \int_x [\nabla \cdot (V_i \nabla S) - \nabla S \cdot \nabla V_i] \, dxdy \qquad \text{III-5}$$

$$= K_h \{ \quad V_i \nabla S \cdot \hat{n} \, dr - \int_y \int_x \nabla V_i \cdot \nabla S \, dxdy \}$$

where $\hat{n}$ is a unit vector normal to the domain and dr is the differential distance along the path of integration on the perimeter of the domain.

The contour integral in III-5 vanishes because $\frac{\partial S}{\partial x}$ cancels out due to cyclic continuity and $\frac{\partial S}{\partial y} = 0$ because there is no flux across the channel walls at the north and south edges of the domain. Using III-3, the remaining term on the r.h.s. of III-5 can be written

$$-K_h \langle \nabla V_i \cdot \nabla S \rangle = - K_h [\langle \frac{\partial V_i}{\partial x} , \gamma_j \frac{\partial V_j}{\partial x} \rangle + \langle \frac{\partial V_i}{\partial y} , \gamma_j \frac{\partial V_j}{\partial y} \rangle] \qquad \text{III-6}$$

Combine III-4 and III-6 into the transformed advection equation as follows

$$\dot{\gamma}_j \langle V_j, V_i \rangle + \gamma_j \{ \alpha_k \langle V_k \frac{\partial V_j}{\partial x} , V_i \rangle + \beta_k \langle V_k \frac{\partial V_j}{\partial y} , V_i \rangle$$

$$+ K_h [\langle \frac{\partial V_i}{\partial x} , \frac{\partial V_j}{\partial x} \rangle + \langle \frac{\partial V_i}{\partial y} , \frac{\partial V_j}{\partial y} \rangle] \} = 0$$

Now using a centered difference in time gives the forecast equation

$$(\gamma_j^{n+1} - \gamma_j^{n-1})\langle V_j, V_i\rangle = -2\Delta t\, \gamma_j^{n}\{\alpha_k^{n} \langle V_k \frac{\partial V_j}{\partial x}, V_i\rangle + \beta_k^{n} \langle V_k \frac{\partial V_j}{\partial y}, V_i\rangle$$

$$+ K_h[\langle \frac{\partial V_i}{\partial x}, \frac{\partial V_j}{\partial x}\rangle + \langle \frac{\partial V_i}{\partial y}, \frac{\partial V_j}{\partial y}\rangle]\} \qquad \text{III-7}$$

when n is the time step. In this model α^n and β^n are not forecast quantities, but are either specified for each time step or are constant. They represent the prescribed wind field which is advecting the scalar S.

This equation is valid for each node i and as such is a matrix equation of the form

$$[A]\ \{x\} = \{b\}$$

where

$[A] = \langle V_j, V_i \rangle$ with dimensions n by n

$\{x\} = (\gamma_j^{n+1} - \gamma_j^{n-1})$ with dimensions n by 1

$\{b\}$ = The right-hand side of III-7 with dimensions n by 1

and n is the number of nodes.

Note that all of the inner products are independent of time so that they need only be calculated once and placed in mass storage to be accessed at each time step.

IV. EVALUATION OF INNER PRODUCTS

Even though the choice of elements in this investigation is triangles with nodes at the vertices, this is by no means the only choice possible. The elements could be triangles with six nodes each; rectangles with six, eight or twelve nodes; or any other polygon or curved-sided element. More complex elements would allow higher orders of continuity. Bathe and Wilson (1976) describe the technique of isoparametric interpolation as applied to the FEM. However, these more complex elements require even more complex formulations. The mathematics can get out of hand very quickly requiring many more terms and complicated integrations. Also Galerkin's method is not the only weighted residual technique available. Crandall (1956) describes the collocation, subdomain, and least squares methods as well. Lower order continuity is deemed to be acceptable in this investigation because the grid resolution is fine enough so that the change in variable is assumed to be linear between grid points. This assumption allows the selection of triangular elements and the Galerkin method, each of which will significantly simplify the mathematics.

Figure 6 shows a typical element with a point p described in area coordinates. Lines are drawn from p to each of the vertices (x_j, y_j, j=1,2,3) dividing the element into the areas A_j (j=1,2,3).

Define: $L_j = A_j/A$

where A = total element area

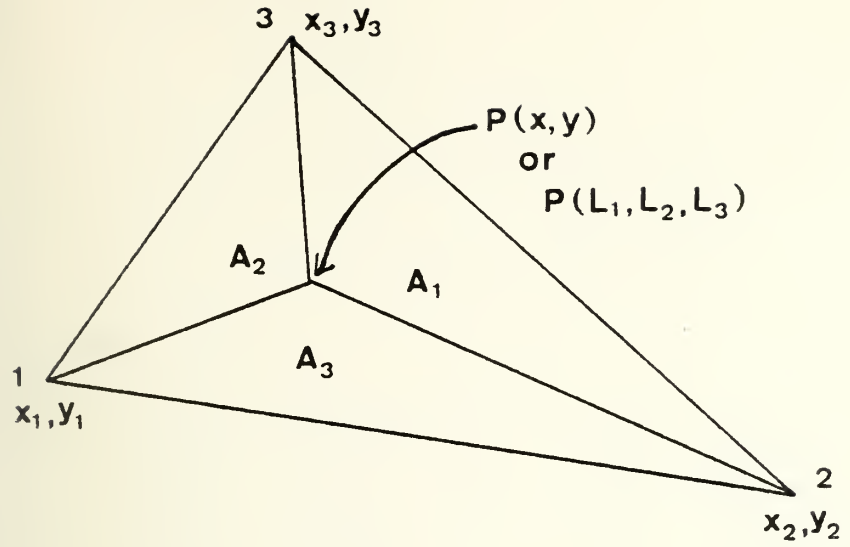

Figure 6. A typical element illustrating the area coordinate system.

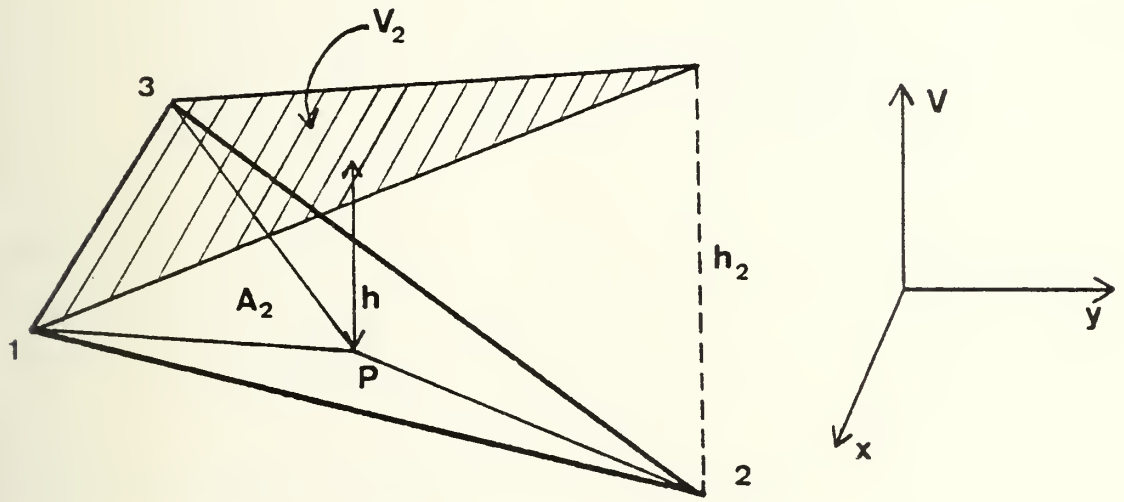

Figure 7. An element with part of a basis function.

Now

$$L_1 + L_2 + L_3 = 1$$

$$x = L_1x_1 + L_2x_2 + L_3x_3$$

$$y = L_1y_1 + L_2y_2 + L_3y_3$$

or, in matrix form

$$\begin{Bmatrix} 1 \\ x \\ y \end{Bmatrix} = \begin{bmatrix} 1 & 1 & 1 \\ x_1 & x_2 & x_3 \\ y_1 & y_2 & y_3 \end{bmatrix} \begin{Bmatrix} L_1 \\ L_2 \\ L_3 \end{Bmatrix}$$

or, solving for the L vector

$$\begin{Bmatrix} L_1 \\ L_2 \\ L_3 \end{Bmatrix} = \frac{1}{2A} \begin{bmatrix} 2A & b_1 & a_1 \\ 2A & b_2 & a_2 \\ 2A & b_3 & a_3 \end{bmatrix} \begin{Bmatrix} 1 \\ x \\ y \end{Bmatrix} \qquad \text{IV-1}$$

where

$$a_1 = x_3 - x_2 \qquad b_1 = y_2 - y_3$$

$$a_2 = x_1 - x_3 \qquad b_2 = y_3 - y_1$$

$$a_3 = x_2 - x_1 \qquad b_3 = y_1 - y_2$$

So that any one of the equations in IV-1 is really

$$L_j = 1 + \frac{b_j}{2A} x + \frac{a_j}{2A} y \qquad \text{IV-2}$$

But by the chain rule

$$\frac{\partial}{\partial x} = \frac{\partial L_j}{\partial x}\frac{\partial}{\partial L_j} = \frac{b_j}{2A}\frac{\partial}{\partial L_j}$$

and IV-3

$$\frac{\partial}{\partial y} = \frac{\partial L_j}{\partial y}\frac{\partial}{\partial L_j} = \frac{a_j}{2A}\frac{\partial}{\partial L_j}$$

where the repeated subscript indicates a summation from one to three.

Consider Figure 7. The heavy black lines outline an element divided into area coordinates defining point P, and only A_2 is labeled. The hatched triangle (labeled V_2) is that part of the basis function associated with node 2 that lies over the element. There are two more basis functions called V_1 and V_3 that are associated with nodes 1 and 3 respectively. Both of these functions also have linear sections over the element. However, they have been omitted from Figure 7 to avoid clutter. The altitude h_2 is defined as unity. The altitude h is the value of V_2 at P. Recall $L_2 = A_2/A$. As P moves from node 2 to the opposite side of the element, h varies linearly from 1 to 0. Following the same path L_2 also varies linearly from 1 to 0. So that at any point P on the element $L_2 = h = V_2$. In general, $L_j = V_j$. This is the first great advantage of triangular elements.

So now, using IV-3

$$\frac{\partial V_i}{\partial x} = \frac{b_1}{2A}\frac{\partial V_i}{\partial L_1} + \frac{b_2}{2A}\frac{\partial V_i}{\partial L_2} + \frac{b_3}{2A}\frac{\partial V_i}{\partial L_3}$$

$$= \frac{b_1}{2A}\frac{\partial L_i}{\partial L_1} + \frac{b_2}{2A}\frac{\partial L_i}{\partial L_2} + \frac{b_3}{2A}\frac{\partial L_i}{\partial L_3}$$

but

$$\frac{\partial L_i}{\partial L_j} = 1 \quad \text{if} \quad i = j$$

$$= 0 \quad \text{if} \quad i \neq j$$

So

$$\frac{\partial V_i}{\partial x} = \frac{b_i}{2A} \quad \text{and similarly} \quad \frac{\partial V_i}{\partial y} = \frac{a_i}{2A} \qquad \text{IV-4}$$

Note that these derivatives are dependent upon the individual elements and are constant with time. Therefore they need only be calculated once and be stored as part of the inner products.

The second great advantage of triangular elements and linear basis functions is the general area integration formula

$$\int_A L_1^m L_2^n \, dA = \frac{m!n!}{(m + n + 2)!} 2A \qquad \text{IV-5}$$

or, rewritten as an example of an inner product:

$$\langle L_1^2, L_2 \rangle = \frac{2!1!}{5!} 2A = \frac{A}{30}$$

Now the inner products for equation III-7 may be rewritten with the aid of IV-4 and IV-5:

$$\langle V_j, V_i \rangle = \langle L_j, L_i \rangle = \frac{1!1!}{4!} 2A = \frac{A}{12} \qquad \text{if } i \neq j$$

$$= \langle L_i^2 \rangle = \frac{2!1!}{4!} 2A = \frac{A}{6} \qquad \text{if } i = j$$

$$\langle V_k \frac{\partial V_j}{\partial x}, V_i \rangle = \frac{b_j}{2A} \langle L_k, L_i \rangle = \frac{b_j}{2A} \frac{A}{12} = \frac{b_j}{24} \qquad \text{if } k \neq i$$

$$= \frac{b_j}{12} \qquad \text{if } k = i$$

$$\langle V_k \frac{\partial V_j}{\partial y}, V_i \rangle = \frac{a_j}{24} \qquad \text{if } k \neq i$$

$$= \frac{a_j}{12} \qquad \text{if } k = 1$$

$$\langle \frac{\partial V_i}{\partial x}, \frac{\partial V_j}{\partial x} \rangle = \frac{b_i}{2A} \frac{b_j}{2A}$$

$$\langle \frac{\partial V_i}{\partial y}, \frac{\partial V_j}{\partial y} \rangle = \frac{a_i}{2A} \frac{a_j}{2A}$$

V. INITIAL AND BOUNDARY CONDITIONS

Simple initial conditions are used for the scalar field S and the wind components u and v. The S field consists of a half sine wave in the y direction and multiple waves in the x direction. These multiple waves are the mechanism used to generate smaller scale features. The $\frac{\pi}{2}$ term in the u equation causes the area of fastest flow to be coincident with the area of highest spatial resolution.

$$S = A \sin\left(\frac{2n\pi x}{L}\right) \sin^4\left(\frac{\pi y}{W}\right) \qquad \text{V-1}$$

$$u = \overline{U} + B \cos\left(\frac{2\pi x}{L} - \frac{\pi}{2}\right) \qquad \text{V-2}$$

$$v = \overline{V} = 0$$

where

A = arbitrary amplitude = 400 meters

n = wave numbers = 1,...,6

L = channel length = 2400 km

W = channel width = 2400 km

$\overline{U}$ = mean zonal wind = 20 m/sec

B = $\overline{U}$ x R; R is the ratio of the perturbation wind to the mean zonal wind

Figures 8 and 9 depict the initial fields of S and u respectively.

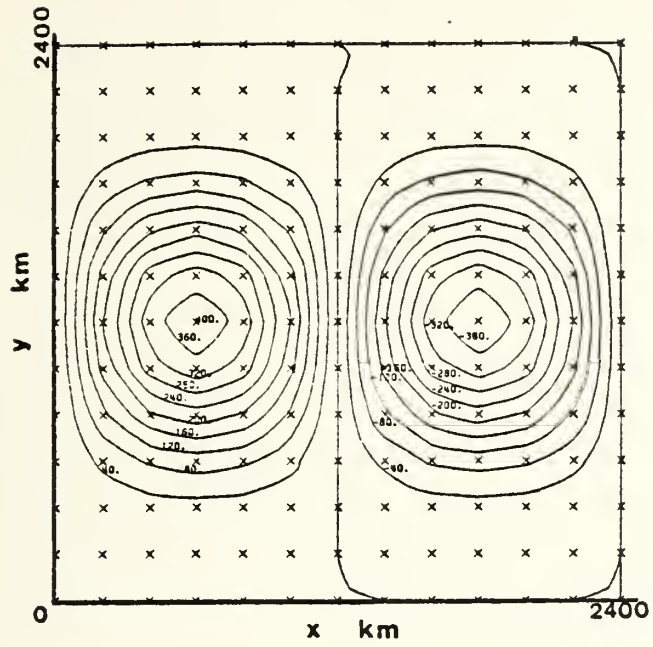

Figure 8. Initial field for the scalar S.

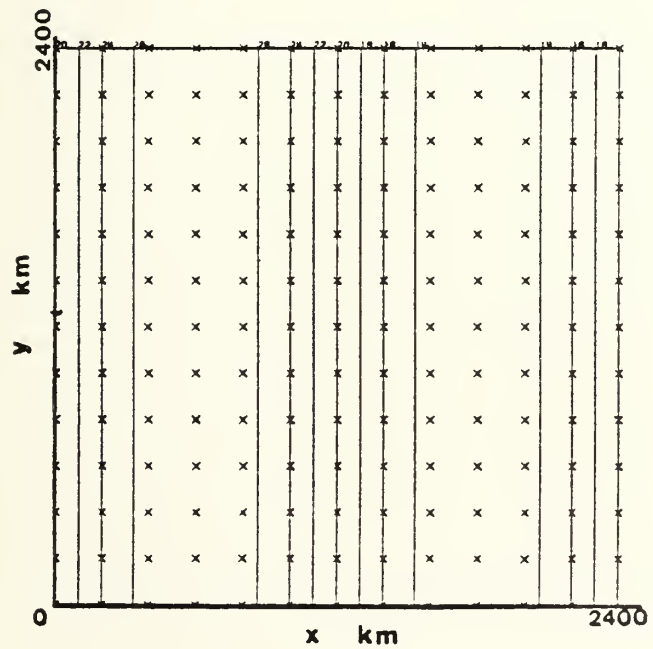

Figure 9. Initial u field with wind ratio R = 0.4.

Boundary conditions are also handled simply. Cyclic continuity is assured in the x-direction by selecting the proper node convectivity. Two techniques are used to control flow across the channel walls at the north and south sides. First, the exponent on the y-component of the initial wave is high enough to keep the value of S close to zero in the vicinity of the walls. Second, the solution method is iterative so that the values of the nodes one row in from the channel walls are set equal to the nodes on the walls at each iteration. The result is that diffusion from the edges into the interior is disallowed.

VI. COMPUTATIONAL TECHNIQUES

A. NUMBERING SCHEMES

As described in Chapter IV, the inner products may be easily evaluated on the individual element level. To facilitate this evaluation, a local numbering system is required for each element. An array called IEL, dimensioned N by 3, contains the identification number of the nodes on the three verticies for each of N elements. For each element these node numbers must be stored sequentially in a positive sense, that is counterclockwise. The node with which to start numbering, however, is arbitrary.

In addition to the local numbering system, a "mass" matrix is needed. The mass matrix is a matrix of coefficients whose rows are the equations of the system to be solved. There is one equation (row) for each node. Each equation will have a term (column) for each node. A non-zero entry in the mass matrix indicates connectivity. That is, if entry (I,J) is non-zero then node I is connected to node J. Two nodes are connected if they are both vertices of the same triangular element. In this model, each node is connected to a minimum of two and a maximum of six or eight other nodes depending upon model version. The model uses an array called MAME dimensioned N by 7 (or 9) that contains the numbers of all nodes connected to any specific node, including itself, for each of N nodes. MAME will contain from 3 to 7 (or 9) non-zero entries in each row.

To save storage space, MAME is next compacted into a one dimensional vector NAME which contains only the non-zero entires of MAME. The utility vectors ISTART(N) and NUM(N) are also constructed in order to decode NAME. ISTART(N) contains the index in NAME of the starting position of the continuity of any node N. NUM(N) contains the length of the connectivity of node N within NAME. As an example of how to retrieve the connectivity of a node, say node 14, from NAME: Let J = ISTART(14) and let K = NUM(14). Then NAME(J) through NAME(J+K-1) contain the connectivity for node 14.

Consider the matrix equation [A] {x} = {b} from Chapter III. It should be clear that [A] is the mass matrix mentioned above. It is a very sparse matrix containing the inner products $\langle V_j, V_i \rangle$ for row j and column i. In this model [A] is compacted into the vector {H} using NAME as a lookup table. The result is that there is no longer a real matrix equation, but rather just the product of vectors

$$\{H\}\ \{x\} = \{b\} \qquad \text{VI-1}$$

B. SOLUTION TECHNIQUE

An advantage of economy of space has been gained, but VI-1 now requires an iterative solution. The solution chosen is a standard Gauss-Seidel technique which requires a reversal of direction of iteration every pass. An average of 16 passes are needed for each time step. The solution is considered to have converged to its final value when:

$$\frac{|x_i^{\ell} - x_i^{\ell-1}|}{x_i^{\ell}} \leq 10^{-6}$$

for every node i.

with: ℓ = iteration number

x_i = solution for node i in x

More efficient solution schemes are available, but this one was selected because of its simplicity. Minimizing computation times is not of high priority to this investigation for two reasons: first, the recently installed IBM 3033 is a fast machine, and secondly, since an advection model doesn't contain gravity waves, stability can be maintained with very large time steps. As an example, a twelve hour forecast with a grid size of 200 km and a time step of one hour requires less than eight seconds of CPU time. Even the largest version of the model with longer forecast length, higher resolution and linkage to the plotting software takes less than eight minutes.

C. ROBERT FILTER

Haltiner and Williams (1980) discuss the advantages of time averaging. Averaging operators act as low-pass filters that tend to remove high frequency waves while having little effect on long-period waves. Even very weak filters will remove high frequency noise if used at every time step. In this model, the choice of filters is that of Robert (1966).

First, assume that an average field $\bar{S}_{n-1}$, already exists at time level n-1 as well as the unaveraged field S_n at time level n. Then the model uses its predictor equation to determine the solution vector {x}. For each node, an unaveraged predicted value is computed as

$$S_{n+1} = \bar{S}_{n-1} + x$$

Next, the corrected values at time n are determined from

$$\bar{S}_n = S_n + \gamma \, (S_{n+1} - 2S_n + \bar{S}_{n-1}) \qquad \text{VI-2}$$

where γ is the averaging coefficient. Finally, $\bar{S}_n$ is stored in place of $\bar{S}_{n-1}$ and the model continues on to the next step.

The value of γ must be carefully chosen as it does effect the computational stability. As γ increases, the maximum time step decreases. Haltiner and Williams prefer a γ less than 0.25 in order to permit a reasonable time step. Additionally, it should be noted that a large value of γ will begin to dampen waves in the meteorological frequency range. On the other hand, Robert used a value of $\gamma = 0.01$ applied over a total forecast length of many days. This very weak filter was all that was needed for noise suppression.

For the model in this investigation γ is an input parameter. For one set of tests in Chapter X, the value of γ is varied from 0.01 to 0.04.

D. DETERMINATION OF TIME STEP

Cullen (1973) calculated the stability criterion for the two-dimensional problem as:

$$\Delta t \leq \frac{\Delta x}{c\sqrt{6}} \qquad \text{VI-3}$$

the minimum grid distance, Δx, varies from 200 km to about 40 km. The propagation speed, c, varies from 40 m/sec to 0. Accordingly, the time step has been chosen as 60 minutes for the coarse mesh versions, and ten or five minutes in the finer mesh versions.

VII. NODAL GEOMETRIES

Once the decision has been made to use triangular elements, the next choice is the type of triangle. This investigation concerns both right and equilateral triangles.

A. RIGHT TRIANGLES

Figure 10 is an example of the right triangle arrangement used in this model for a uniform grid. The domain is divided into a series of rectangles, and then each rectangle is bisected by a diagonal to form a pair of triangles. Kelly and Williams found that significant bias was introduced into the model if all of the diagonals sloped in the same direction. This model overcomes that kind of bias by alternating the slope of the diagonals from rectangle to rectangle both horizontally and vertically. Consequently, the connectivity of the nodes will vary from four to nine total connections, and each node connects with itself.

Two methods are used to vary the grid resolutions with right triangles. In the first method a FORTRAN DATA statement specifies coefficients used in the calculation of the nodal coordinates. This method is very simple and has the advantage of keeping all the nodes in a rectangular arrangement. Rectangularly arranged nodes lend themselves well to harmonic analysis with some interpolation. The grid may be varied in either one or both the x and y-directions. Figure 11 is an example of the nodal arrangement by this method with variation in both

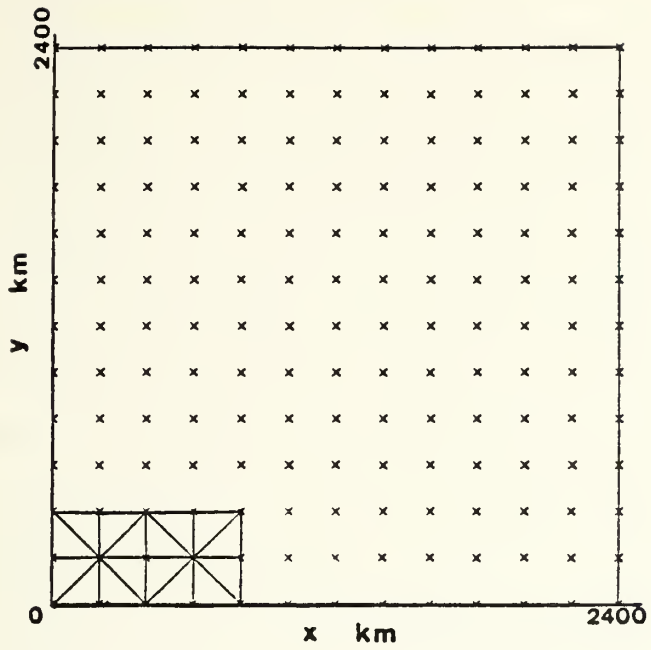

Figure 10. The domain divided into right triangular elements. Only the elements in the lower-left corner are drawn, but the pattern is repetitive over the entire domain. Each node is marked with an 'X'.

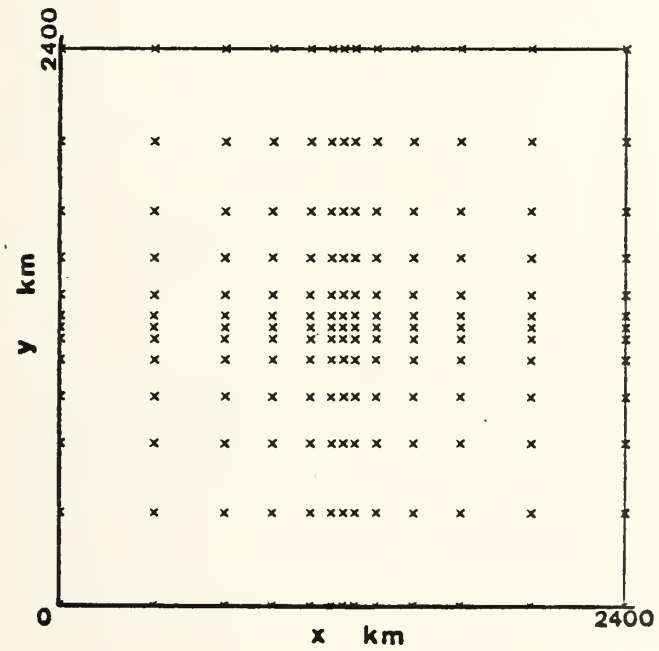

Figure 11. Same as figure 10 with non-uniform elements.

directions. The disadvantage here is that the resolution must be kept relatively fine in parts of the domain away from the area of interest (the center). Optimumly, the resolution should be fine about the area of interest and more coarse elsewhere, hence the next method.

In the second method, the domain is divided into quadrants with the origin at the center of the domain. The nodes around the outer boundary of the first quadrant are specified as having the same coordinates as the uniform grid. But the nodes along the abscissa and ordinate are compressed toward the origin by the use of another DATA statement. Consider four nodes each with coordinates (x_i, y_i), $i = 1...4$. Node 1 is on the ordinate, node 2 on the right boundary, node 3 on the abscissa, and node 4 on the top boundary. The line from node 1 to 2 is defined by

$$\frac{y - y_1}{x - x_1} = \frac{y_2 - y_1}{x_2 - x_1} \qquad \text{VII-1}$$

And the line connecting nodes 3 and node 4 is

$$\frac{y - y_3}{x - x_3} = \frac{y_4 - y_3}{x_4 - x_3} \qquad \text{VII-2}$$

Equations VII-1 and VII-2 are then solved simultaneously to calculate the coordinates of the node located at the intersection of the two lines. By selecting the proper pairs of nodes along the boundaries and axes, the coordinates of all the nodes on the interior of the first quadrant are

found by VII-1 and VII-2. The nodes about the origin are then slightly adjusted to allow local uniformity. Finally the first quadrant is reflected about the axes to form the other three quadrants in the domain. Figure 12 is an example of such an arrangement.

The advantage of this method is that the resolution is fine only in the area of interest, and changes smoothly in all directions away from that area. The disadvantages are the complexity and the non-rectangularity of the nodes.

B. EQUILATERAL TRIANGLES

Preliminary results of the model indicated the presence of a degree of noise when using right triangles. Cullen (personal conversation) suggested the use of equilateral triangles as an alternative element arrangement. Figure 13 is an example of such an arrangement. The right triangles along the sides of the domain are in reality halves of equilateral triangles. Because of cyclic continuity, the domain actually "wraps around" so that all of the elements are equilateral. Note that the maximum connectivity is now only seven and that the domain is no longer square but rectangular.

Variation of resolution is now somewhat more complicated and is accomplished by a transformation of coordinates. The desired end is a smooth and easily controllable stretchage and shrinkage of the coordinate axes. In the x-direction, the transformation is

$$X = x + a \cos kx \qquad \text{VII-3}$$

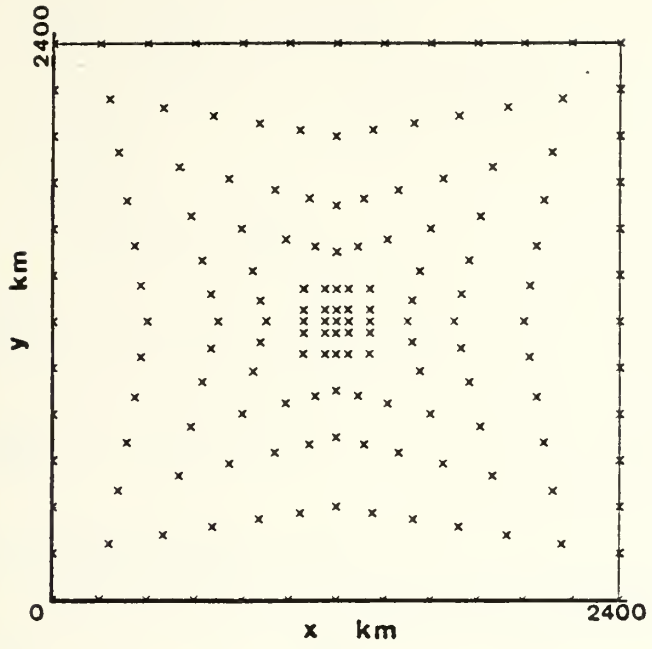

Figure 12. An alternate method of varying resolution.

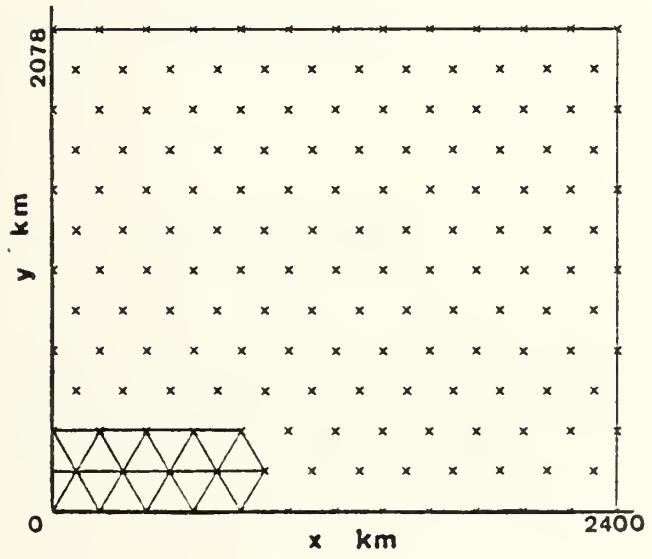

Figure 13. Same as figure 10 except with equilateral triangular elements.

where X = transformed coordinate

x = original coordinate

a = coefficient to be determined

$k = \frac{2\pi}{L}$

L = channel length

the map factor $\frac{\partial X}{\partial x}$ is defined by

$$\frac{\partial X}{\partial x} = 1 - ak \sin kx$$

whose maximum and minimum values are

$$\left(\frac{\partial X}{\partial x}\right)_{max} = 1 + ak \; ; \; \left(\frac{\partial X}{\partial x}\right)_{min} = 1 - ak$$

The ratio, r_1, of maximum stretch to minimum shrink is

$$r_1 = \frac{1 + ak}{1 - ak}$$

or, solving for a

$$a = \frac{r_1 - 1}{k(r_1 + 1)} \qquad \text{VII-4}$$

To keep the transformed coordinate system from folding back on itself, a must be positive. That is, r_1, must be equal to or greater than one.

Variation of resolution is accomplished by selecting an appropriate value for r_1 and then substituting equation VII-4 into VII-3. Similar expressions can be derived for the transformation of the y-coordinate by the use of the ratio r_2.

The advantage of this method is the extremely sensitive control upon resolution afforded by the ratios r_1 and r_2. Once programmed, this method is much easier to use than the more cumbersome DATA statements of the previous methods. The major disadvantage is that the transformed system is no longer made up of equilateral triangles if one of the ratios is different than one. Figure 14 is the nodal arrangement with $r_1 = 5$ and $r_2 = 3$.

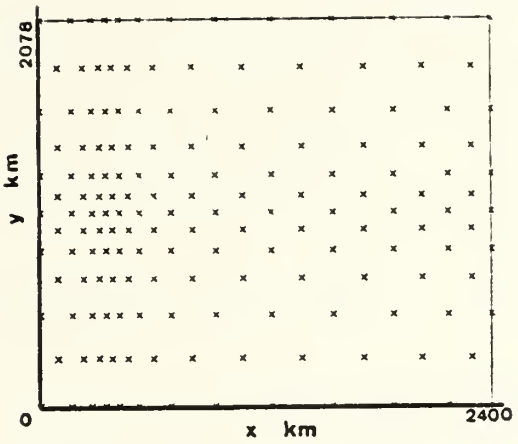

Figure 14. Same as figure 13 but $r_1 = 5$, $r_2 = 3$.

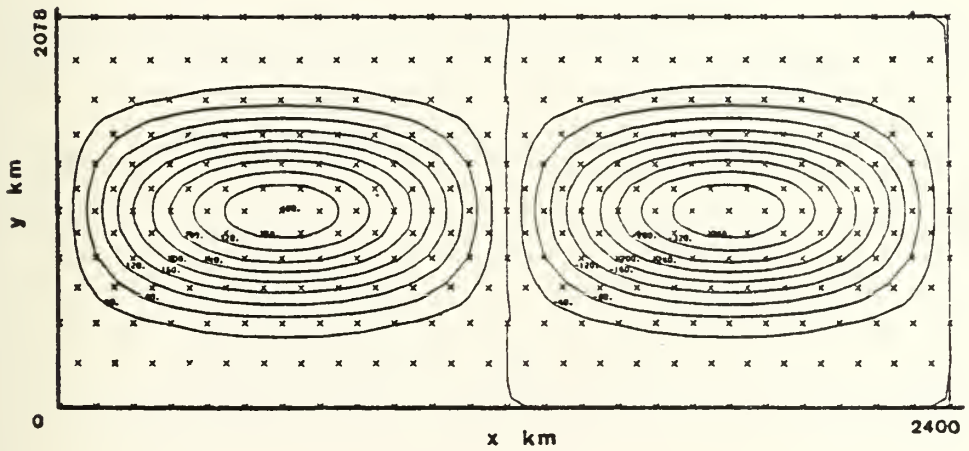

Figure 15. Initial S field for the diffusion tests.

VIII. FORCING TERM

As part of an effort to improve the testing of a numerical scheme, it is often beneficial to force the scheme with the desired solution, if known. Since this model is a simple advection scheme, the output will look very similar to the initial condition.

Assume the solution is of the form

$$S = \cos\,[\mu(X - \lambda t) + \delta]$$

where

$$\mu = \frac{2\pi}{Lx},$$

λ = phase speed,

$$\delta = -\frac{\pi}{2},$$

X = transformation of x coordinate.

If v = 0, then the forced advection equation is

$$\frac{\partial S}{\partial t} + u\,\frac{\partial S}{\partial x} = F(x,t) \qquad \text{VIII-1}$$

but

$$\frac{\partial S}{\partial t} = \mu\lambda\,\sin[\mu(X - \lambda t) - \frac{\pi}{2}] \qquad \text{VIII-2}$$

and

$$\frac{\partial S}{\partial x} = -\mu\,\frac{\partial X}{\partial x}\,\sin[\mu(X - \lambda t) - \frac{\pi}{2}] \qquad \text{VIII-3}$$

Substituting VIII-2 and VIII-3 into VIII-1

$$\mu(\lambda - u \frac{\partial X}{\partial x}) \sin[\mu(X - \lambda t) - \frac{\pi}{2}] = F(x,t)$$

which is equivalent to

$$\mu(\lambda - u \frac{\partial X}{\partial x}) [\sin(\mu X - \frac{\pi}{2}) \cos(\mu\lambda t) - \cos(\mu X - \frac{\pi}{2}) \sin(\lambda\mu t)] = F(x,t)$$

applying Galerkin's technique this equation eventually reduces to:

$$(f_j - g_j) \langle V_j, V_i \rangle = F(x,t) \qquad \text{VIII-4}$$

where

$$f_j = \mu(\lambda - u \frac{\partial X}{\partial x}) \sin(\mu X - \frac{\pi}{2}) \cos \mu\lambda t$$

$$g_j = \mu(\lambda - u \frac{\partial X}{\partial x}) \cos(\mu X - \frac{\pi}{2}) \sin \mu\lambda t \qquad \text{VIII-5}$$

Now, VIII-4 should be included on the r.h.s. of the predictor equation III-7. Notice that both of the equations VIII-5 contain a time dependent part. The technique now is to calculate the time independent coefficients of VIII-5 at the onset and store them for the duration of program execution. During the forecast sequence, at each time step, the time dependent parts of VIII-5 are calculated, multiplied by the applicable pre-stored coefficients and then assembled into the mass matrix as indicated by VIII-4.

This forcing term will not be used in most of the model runs as a standard part of the predictor equation, but will be the subject of a specific set of tests designed to determine its contribution to forecast accuracy.

IX. ANALYTIC SOLUTION

Consider the one dimensional equivalent of equation III-1 with no diffusion:

$$\frac{\partial S}{\partial t} + u(x) \frac{\partial S}{\partial x} = 0 \qquad \text{IX-1}$$

where flow is zonal only and the velocity may vary spatially. Recall from Chapter V that the zonal wind equation is

$$u(x) = \overline{U} + B \cos(kx - \frac{\pi}{2}) \qquad \text{IX-2}$$

where $k = \frac{\partial \pi}{L}$, L = zonal wave length.

In a simple one dimensional advection equation for any time t, the following holds:

$$S(x,t) = S(x_0, 0)$$

where x_0 is some point upstream in the initial field. Now if x_0 can be determined as a function of the current location and the elapsed time, then the analytic solution for the forecast at that time would be achieved. That is,

$$x_0 = F(x,t)$$

Since $u = \frac{dx}{dt}$, then from IX-2

$$\frac{dx_0}{dt} = \bar{U} + B \cos(kx_0 - \frac{\pi}{2})$$

Integrating

$$\int_{x_0}^{x} \frac{kdx_0}{\bar{U} + B \cos(kx_0 - \frac{\pi}{2})} = \int_{o}^{t} kdt$$

With the help of a Table of Integrals, this expression is evaluated as

$$\frac{2}{(\bar{U}^2 - B^2)^{1/2}} \{\tan^{-1}[\frac{(\bar{U}-B)\tan\frac{1}{2}(kx - \frac{\pi}{2})}{(\bar{U}^2 - B^2)^{1/2}}]$$

$$- \tan^{-1}[\frac{(\bar{U}-B)\tan\frac{1}{2}(kx_0 - \frac{\pi}{2})}{(\bar{U}^2 - B^2)^{1/2}}]\} = kt$$

Let

$$r = \frac{\bar{U} - B}{(\bar{U}^2 - B^2)^{1/2}}$$

So that

$$\tan^{-1}[r \tan\frac{1}{2}(kx - \frac{\pi}{2})] - \tan^{-1}[r \tan\frac{1}{2}(kx_0 - \frac{\pi}{2})] = \frac{1}{2}(\bar{U}^2 - B^2)^{1/2} kt$$

Solving for x_0

$$x_0 = \frac{\pi}{2k} + \frac{2}{k} \tan^{-1} \left\{ \frac{1}{r} \tan \left[\tan^{-1} \left(r \tan \frac{1}{2}(kx - \frac{\pi}{2}) \right) - \frac{1}{2}(\bar{U}^2 - B^2)^{1/2} kt \right] \right\} \quad \text{IX-3}$$

The analytic solution at time t for any node at coordinates (x,y) is found by substituting x and t into IX-3 to obtain x_0. Then x_0 and y are substituted into equation V-1. This process requires each value of x to be operated upon by five trigonometric functions, each of which further compounds truncation error. As a result, this subroutine must be run in double precision. Even so, there is still some small error in the analytic solution field. This investigation is concerned with the relative errors of various nodal arrangements and is not intended for comparison studies between finite element and other methods. Since the errors in all test cases are relative to the same solution, the small error in the solution is not considered significant.

X. RESULTS

The model contains eight variables: element type (equilateral and right triangles), east-west resolution, north-south resolution, wave number, diffusion, Robert filter, uniformity of flow, and number of nodes on the domain. Additionally, the time step may be varied and the initial conditions may be changed so that sharper waves are created. If all of these variables were tested throughout their meteorological range, and if all the interactions between the variables were investigated, the number of computer runs required would be well over ten thousand. Since that many runs is not practical, decisions have to be made concerning the scope of this investigation. There seems to be one of two ways to proceed:

1. One or two questions could be answered rather exactly with an attempt to quantify the relationship between only a couple of variables.

2. General answers can be attempted for many more questions with the aim to set qualitative guidelines for future finite element studies.

In the first alternative above, quantitative relationships would be of little value unless they could be extended to FEM models as a class. Proof that such an extension is valid is clearly beyond this investigation. As a result, the second alternative is chosen and only rather general questions are qualitatively answered.

The model is run a total of 137 times. The runs are compared and contrasted in a number of test cases. Several test cases comprise the

investigation of each question. Two types of statistics are calculated for each run. First of all, a harmonic analysis is accomplished using nodes along each latitude circle, for the initial condition, the forecast field and the analytic solution field. Since the analysis requires equally spaced values, there is an interpolator that calculates values at specific points. The linearity of the basis functions lends itself very well to linear interpolation. One subroutine determines in which element any particular interpolation point lies. Another routine uses the coordinates of that point and the values at the nodes of the proper element to calculate the interpolated value. In the runs that include the forcing term (see Chapter VII), the interpolater is disconnected and the raw nodal values are used. This harmonic analysis generated amplitude and phase information for all possible wave numbers. In the following paragraphs the term"phase speed" denotes the ratio of the phase shift of the forecast wave to the phase shift of the wave in the analytic solution.

The second type of statistics generated considers the forecast and solution values as an ordered pair for each node. A root-mean-square-error (RMSE), correlation and bias are calculated for this set of pairs. By-products of these statistics that are not referred to hereafter are the applicable means and standard deviations.

The following sections are organized such that each one addresses an individual problem, question or technique. To this end, within each section, one or more of the eight variables listed above is varied from a standard or nominal model configuration. Changes in the generated

statistics are then attributed to the influence of the altered variables. The nominal model configuration follows: equilateral elements, uniform grid ($r_1 = r_2 = 1$, see Chapter VII), wave number one, no diffusion, Robert filter, $\gamma = 0.1$, wind perturbation ratio R = 0.0 (see Chapter V), number of nodes = 13 X 12. The standard forecast length is 48 hours, during that period any feature, moving with the mean flow, should move 3456 km or around the domain 1.44 times. Section A is a general statement based upon nearly all of the runs. It includes changes made to all of the variables. In all of the remaining sections, the departure from the nominal configuration is annotated.

A. ACCURACY VS. RESOLUTION

For this test, six runs are discarded because they are deliberately constructed to test unique factors discussed later. In the other 131 runs, the forecast values stay within reasonable limits for all combinations of resolution. In general, the accuracy over the domain as a whole decreases as the stretch of the grid resolution increases, but the statistics all remain bounded. The correlations are all above 0.96, the phase speeds are within four percent and the RMSE is always less than eight percent of the range of the amplitude. Typical values are correlation 0.99, phase speed 1.008 and RMSE one percent of range.

This result is very encouraging in that no cases have to be disregarded simply because they can not be explained. The cases are consistent with one another and exceptions are few.

B. EFFECT OF DIFFUSION

A particularly noisy case is used for this test. The domain length scale has been doubled so that the non-uniform wind is more obvious. With resolution of $r_1 = 1$, $r_2 = 2$ wind perturbation ratio R = 0.4, and 13 X 24 nodes, the diffusion values are incrementally increased from zero. A total of eight runs are made. Figure 15 is the initial condition for this test and Figure 16 is the 48 hour forecast with no diffusion. As diffusion is increased the reduction in RMSE is dramatic and the correlation increases, but the wave amplitude diminishes and the maximum time step must be decreased to insure stability. However, a critical point is eventually reached at which the amplitude is reduced so much that the RMSE starts to climb again and correlation falls. Figure 17 is the 48 hour forecast with the value of diffusion that nearly minimizes the RMSE. Note the absence of noise but the obvious loss of amplitude. Compare this with Figure 18, the analytic solution. Notice that the contour packing is downstream of the high in Figures 16 and 18, but upstream of the high in Figure 17. This reversal of packing is a by-product of the manner in which the model applies diffusion. Cullen (personal communication) suggests that diffusion be increased in the areas of fastest flow and decreased where the flow is slower. Following this advice, the model applies diffusion proportional to the windspeed at each node. The effect with non-uniform flow is that diffusion is also non-uniform, hence the slight alteration in the forecast field. Diffusion appears to be a very effective noise filter, but tests must be made independently for each configuration because the useful limit of diffusion will vary with nodal geometry.

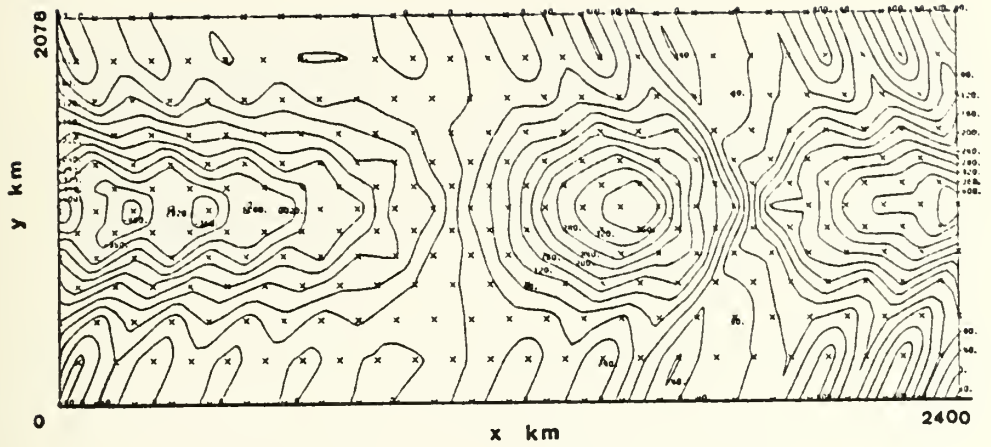

Figure 16. 48 hour forecast for field in figure 15 with no diffusion.

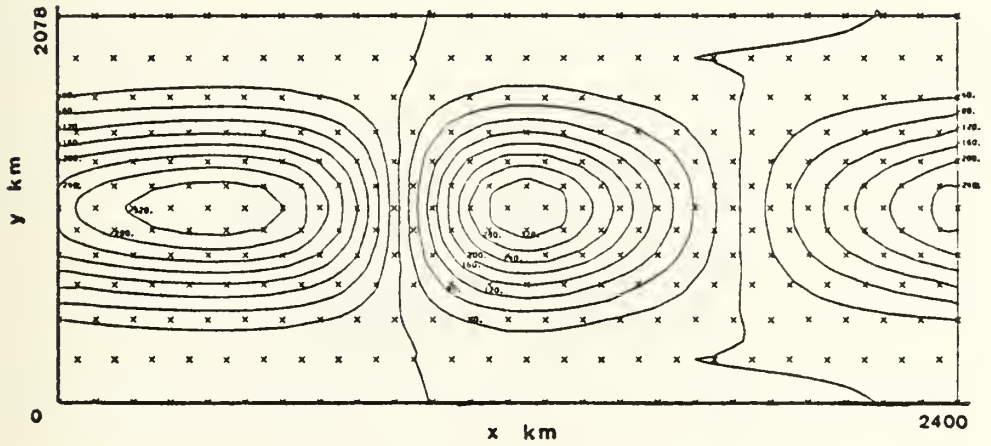

Figure 17. Same as figure 16 but with optimum diffusion.

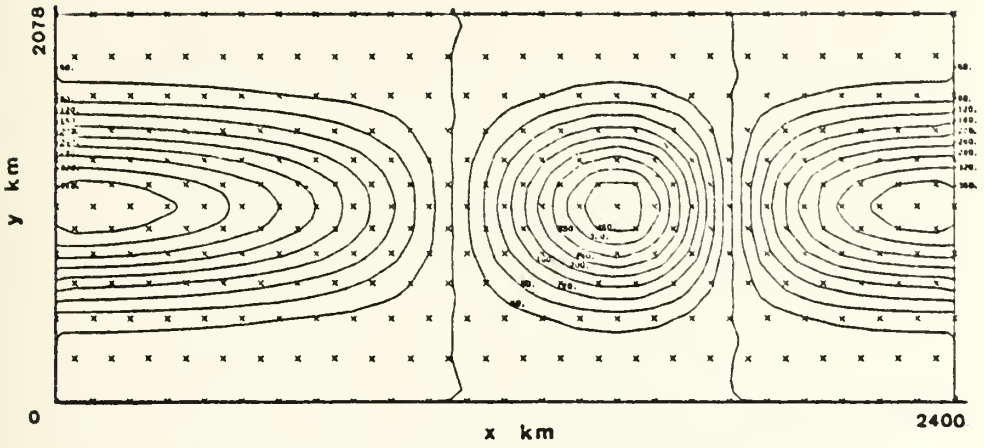

Figure 18. Analytic solution for diffusion tests.

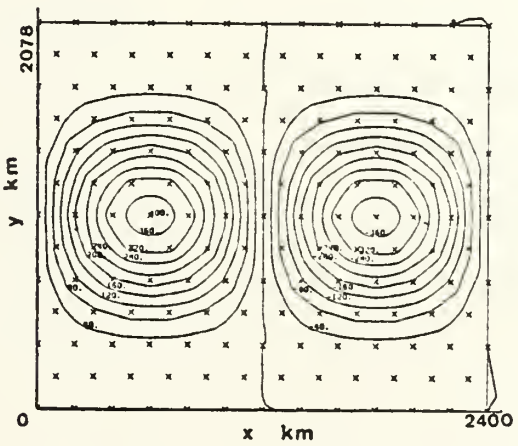

Figure 19. Initial S field for Robert filter tests.

C. EFFECT OF ROBERT FILTER

For this test the model is configured nominally to maximize the accuracy of the solution. The only variable that is changed is the Robert averaging coefficient. Figure 19 is this initial configuration. The averaging coefficient, γ starts at a value of 0.4 and is slowly decreased to 0.01 over 11 runs. The RMSE decreases from 8.7 to 1.74 over this range with a corresponding increase in correlation and the phase speed approaches unity.

Since the filter is desirable to control high frequency noise, a compromise must be reached that will not unduly degrade the forecast. For the rest of this investigation a coefficient of $\gamma = 0.1$ is used since the associated RMSE is only 2.54. Figure 20 is the 48 hour forecast field with this coefficient and Figure 21 is the corresponding analytic solution. There is little improvement in RMSE left to be realized if any effective filtering is desired.

D. ACCURACY VS. WAVE NUMBER

Again the model is configured nominally, except that the number of nodes is 13 X 24. Six runs are made with the wave number varying from one to eight. One would expect the forecast to deteriorate as the wave number increases. This is due in part to the fewer number of nodes along a latitude circle available to resolve each wave. But the deterioration of RMSE is primarily the result of the displacement error measured in terms of the wavelength. A small displacement error with a short wave would produce a much greater deviation from the true solution than would be produced by the same displacement error in a long wave.

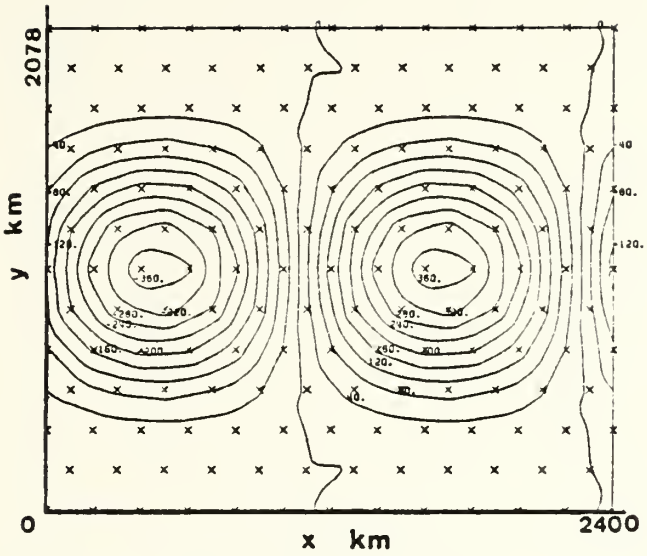

Figure 20. 48 hour forecast for field in figure 19.

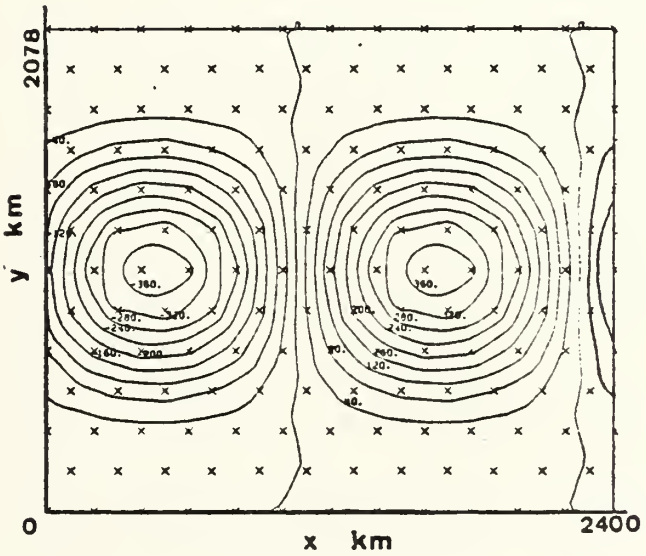

Figure 21. Analytic solution for Robert filter tests.

The results of this test verifies this reasoning. As the wave number of the initial field increases the RMSE worsens, even though the phase speed error stays within four percent. Four of these cases were excluded from Section A above.

Wave Number	Phase Speed Ratio
1	1.008
2	1.008
3	1.02
4	1.03
5	1.04
8	1.03

E. RIGHT TRIANGLES VS. EQUILATERAL TRIANGLES

Five pairs of runs are used to test the hypothesis that elements formed by equilateral triangles yield forecasts superior to those based upon elements formed by right triangles. In all cases the flow is uniform but the resolution is varied among the cases from uniformity to variations in either or both directions. Partial results appear in Table I as Cases 1 through 5. Figures 22, 23 and 24 are the initial field, 48 hour forecast and analytic solution, respectively for the right triangles in Case 3. Figures 25, 26 and 27 are the corresponding figures for equilateral triangles also in Case 3.

The differences between the two arrangements, while not dramatic, are significant and consistent. In every case the RMSE is lower and correlation higher for equilateral triangles. The average reduction in RMSE is about 20 percent. Not shown in Table I but readily apparent in

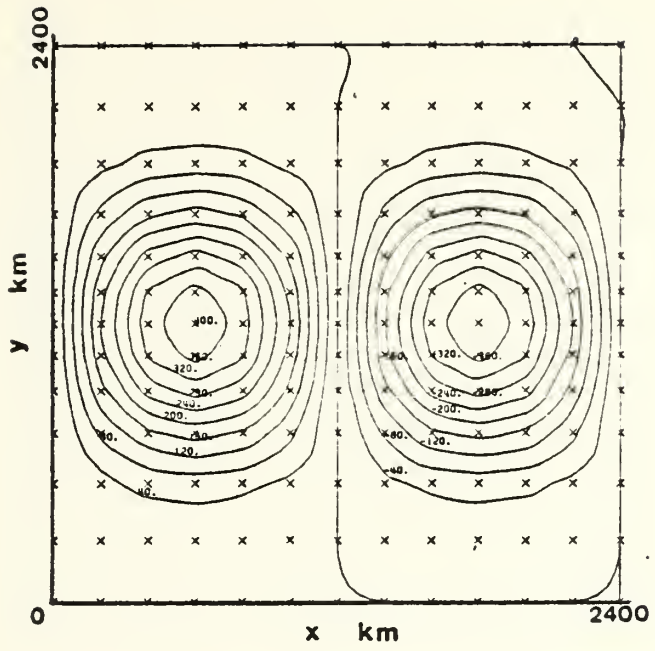

Figure 22. Initial S field for Case 3 with right triangles.

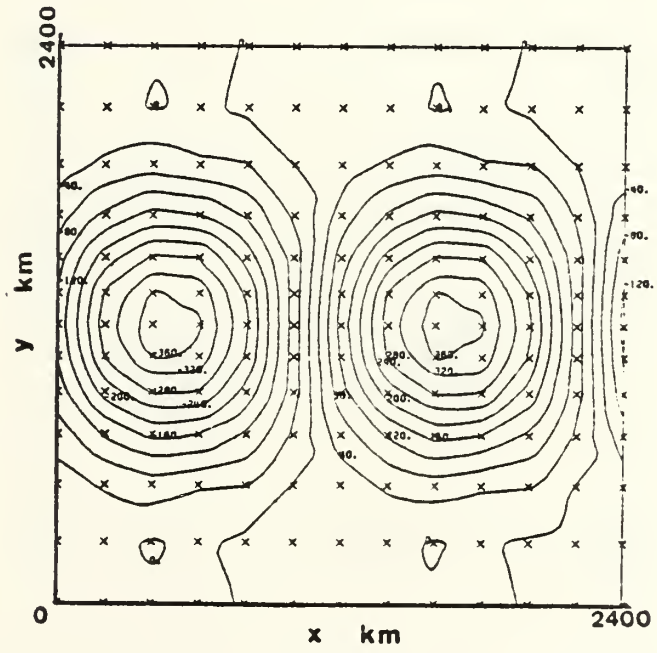

Figure 23. 48 hour forecast for field in figure 22.

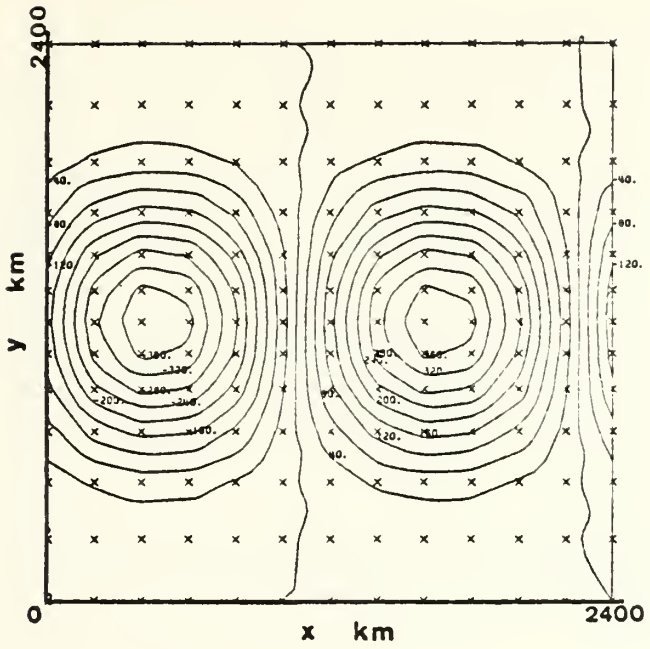

Figure 24. Analytic solution corresponding to figure 23.

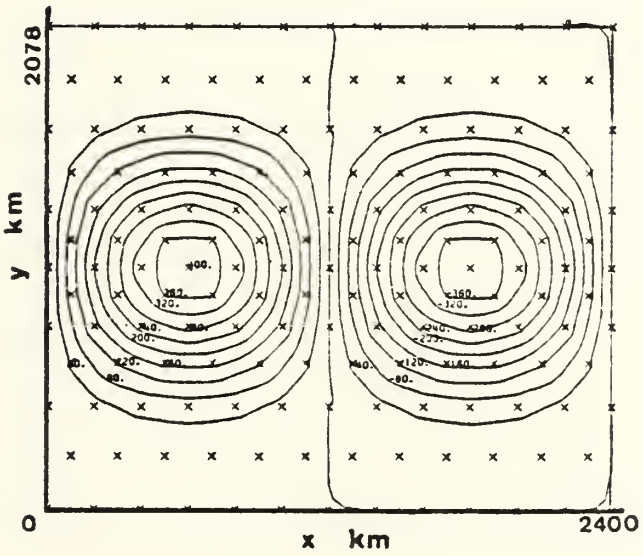

Figure 25. Initial S field for Case 3 with equilateral triangles.

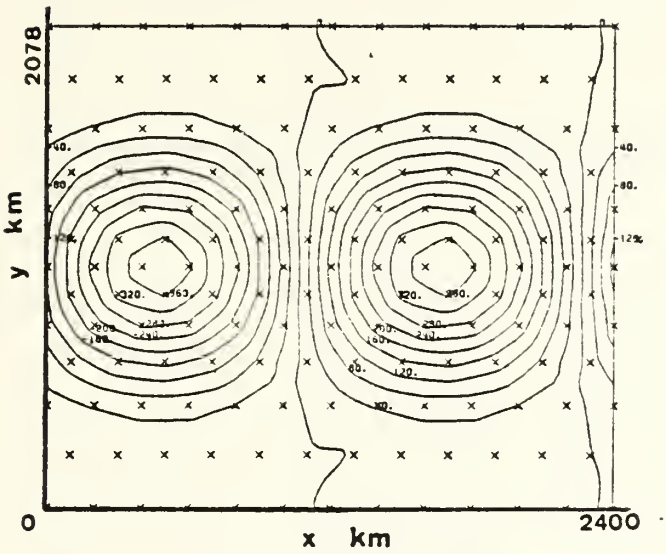

Figure 26. 48 hour forecast for field in figure 25.

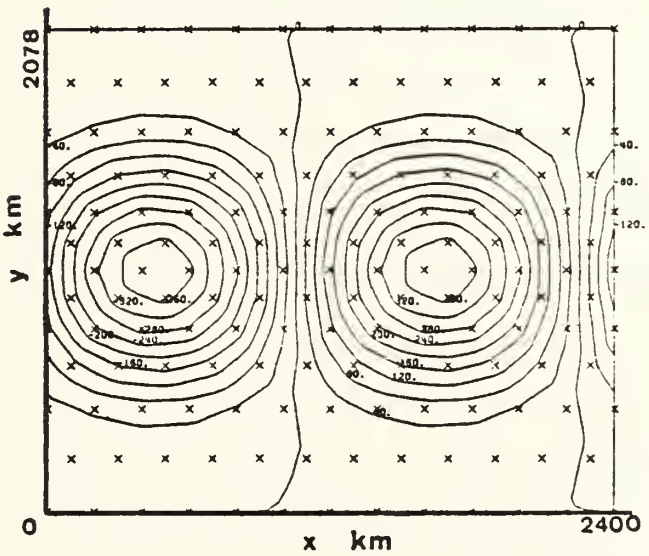

Figure 27. Analytic solution corresponding to figure 26.

the harmonic analysis, is the generation of a spurious wave number five in the right triangle arrangement in four of the five cases.

TABLE I

RESULTS OF RIGHT VS. EQUILATERAL ELEMENT AND DIRECTION OF FLOW TESTS

			RIGHT		EQUILATERAL	
CASE	r_1	r_2	RMSE	CORR.	RMSE	CORR.
1	1	1	4.25	.9994	2.54	.9999
2	2	1	4.54	.9993	4.17	.9996
3	1	2	6.40	.9991	4.87	.9996
4	2	2	6.96	.9990	5.60	.9994
5	3.55	1	6.19	.9981	5.75	.9992
6	1	4	7.48	.9980		
7	4	4	6.60	.9990		
8	1	3.55	9.00	.9980		

F. EFFECT OF ADDING NODES

Next, 16 runs are combined to form nine test cases in order to determine the effect that adding nodes has on the accuracy of the forecast. In this section, the variables are wave number, resolution and number of nodes. It is found that where the model does very well (long waves, uniform flow, relatively small difference in resolution over the entire domain), the addition of more nodes does not increase the accuracy, especially if the additional nodes destroy the original equilateral triangularity. However, if the nodes are added symmetrically in both the north-south and the east-west direction, so that the effect is to increase the resolution uniformly while preserving equilateral triangularity, then the result is an improved forecast.

On the other hand, when the model is initialized with shorter waves, more nodes will improve the forecast even though they may not be added symmetrically. The major advantage of additional nodes is that they allow the resolution to be changed more slowly and more smoothly while attaining a desired minimum resolution. The arrangement with fewer nodes requires a faster and more abrupt resolution change in order to attain the same minimum resolution. The smoothness of the transition between maximum and minimum resolution is apparently the critical factor. Later paragraphs also address this factor. The phase speed ratios for the uniform grids are as follows:

Nodes	Wave Number	Phase Speed Ratio	RMSE
13 x 12	1	1.001	2.5
13 x 24	1	1.008	10.4
25 x 24	1	1.003	7.4
13 x 12	2	1.003	60.29
13 x 24	2	1.002	30.7
25 x 24	2	1.003	25.27

G. VARIATION OF RESOLUTION VS. DIRECTION OF FLOW

The initial conditions for the model are deliberately set to allow only zonal flow. (See Chapter V.) One of the reasons for this is to be able to specifically test the effects of variation of resolution along the direction of flow. A total of 13 runs form six test cases. Many of these runs are the same ones as used in tests in preceding paragraphs. Some of these cases appear in Table I. In that table the comparisons are now vertical. For example, compare Cases 2 with Case 3 to determine that $r_1 = 2$ and $r_2 = 1$ is superior to $r_1 = 1$ and $r_2 = 2$ for both right

and equilateral triangles. This means that varying the resolution with the flow is superior to varying across it. Case 2 is illustrated in Figures 28 and 29 which are the initial field and 48 hour forecast respectively. They should be compared with Figures 25 and 26 which, as stated previously, are part of Case 3. The same result holds for every case on the table. Additional tests have also been run with resolution ratios of six and eight. The results are the same.

One further test can be conducted with the data on Table I. Resolution ratios of $r_1 = r_2 = 2$ will yield the same overall resolution as one of the ratios equal to 3.55 and the other unity. This is the rational for Cases 4, 5 and 8. These cases show that better results can be obtained by varying resolution in both directions as opposed to only across the flow by an equivalent amount. This fact agrees with the results of the previous section in that varying resolution in both directions tends to maintain the equilateral triangularity better than varying across the flow alone.

H. SMOOTH VS. ABRUPT VARIATION OF RESOLUTION

For this test, a version of the model is employed that allows the resolution to be changed abruptly. That version is paired with a more standard version that allows smoother variation of resolution. Both versions use right triangular elements. Both versions generate the same maximum resolution, but with very different transitions to the area of coarser mesh. Twelve runs are paired into six tests. Two different wave numbers and three kinds of flow are tested. These runs included

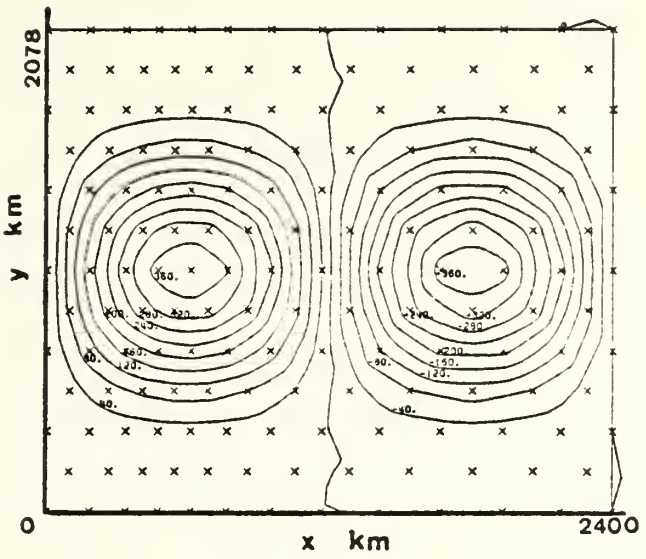

Figure 28. Initial S field for Case 2.

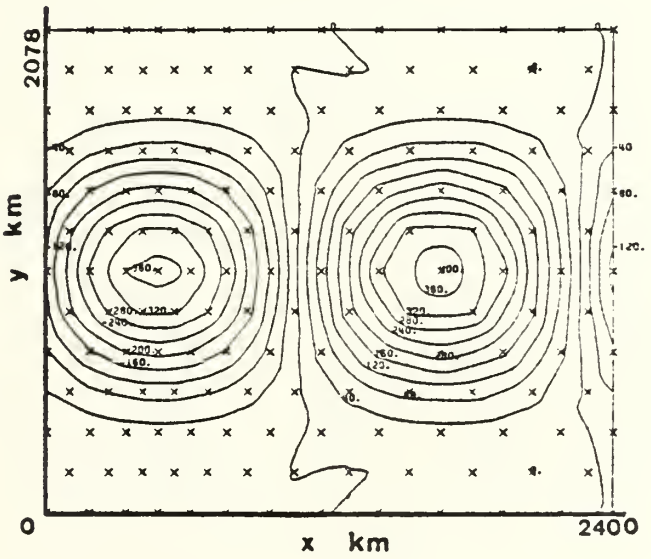

Figure 29. 48 hour forecast for Case 2.

both the normal and "flipped" (See Section J below) configuration. The results are contained in Table II. Even though only six tests are used, the results are dramatic and highly significant. The reduction in RMSE from the abrupt to the smooth cases averages 62 percent. Although not shown, the reduction in bias averages 70 percent. Additionally the abrupt cases generate significantly more noise at all frequencies. Cases 10 and 12 are the last two cases excluded from Section A above. Figures 30 through 33 illustrate the evolution of the forecast in Case 9. The figures are the initial field and 12, 24 and 48 hour forecast respectively for the abrupt change. Compare these to Figures 34 and 35 which are the initial field and 48 hour forecast for the corresponding smooth change.

Combining this result with that of Section F above, it is obvious that the model is highly sensitive to the rate and smoothness of the transition from fine to coarse resolution.

TABLE II

RESULTS OF SMOOTH VS. ABRUPT TESTS

	WAVE	WIND	SMOOTH		ABRUPT	
CASE	NUMBER	RATIO	RMSE	CORR.	RMSE	CORR.
9	1	0.0	4.54	.999	13.6	.989
10	2	0.0	28.3	.956	89.2	.470
11	1	0.2	9.46	.996	23.5	.968
12	1	0.4	21.4	.979	39.9	.895
11F	1	0.2	4.53	.999	14.6	.987
12F	1	0.4	8.83	.996	20.0	.979

I. EFFECT OF VARIABLE WINDS

In several of the previous tests, reference has been made to non-uniform flow. For this section and the following two sections a total

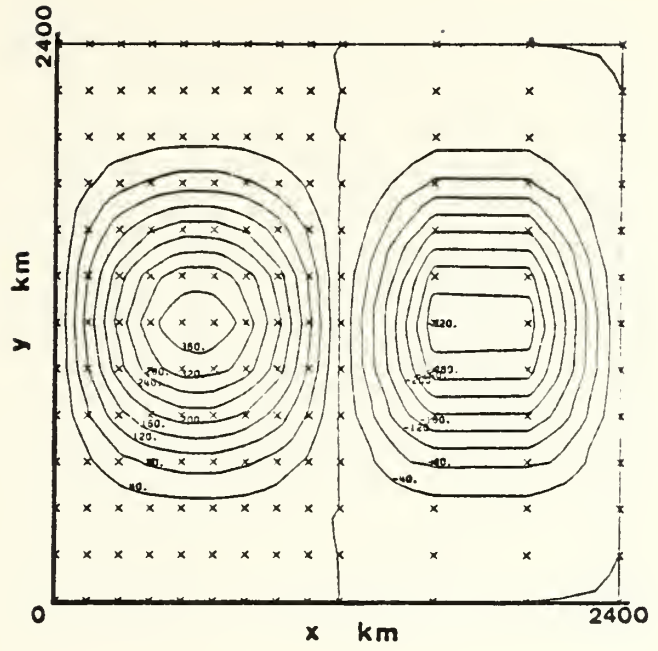

Figure 30. Initial S field with abrupt change of resolution (Case 9).

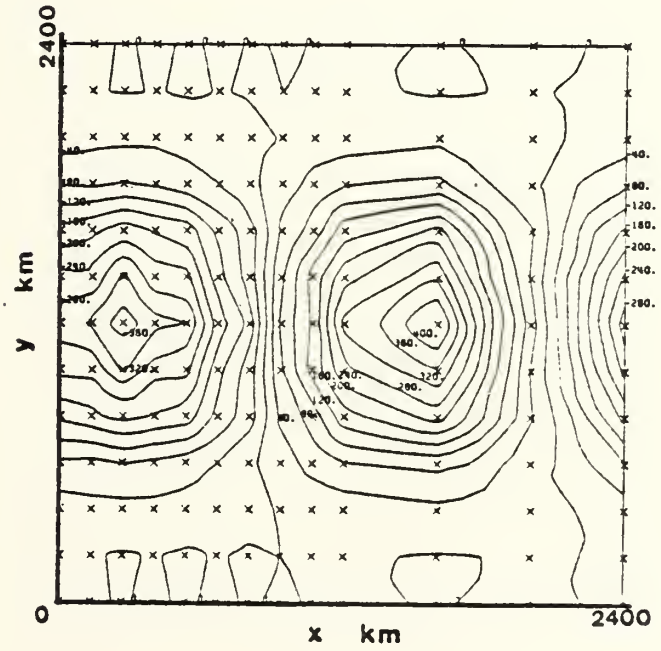

Figure 31. 12 hour forecast for field in figure 30.

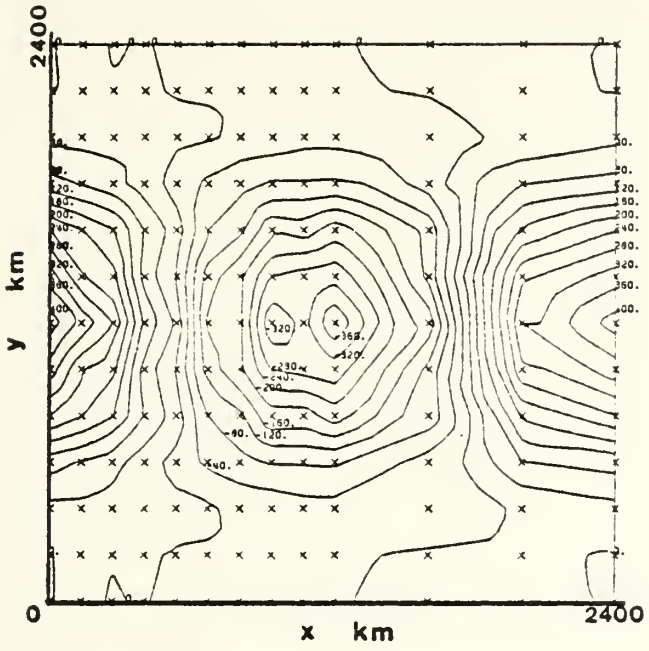

Figure 32. 24 hour forecast for field in figure 30.

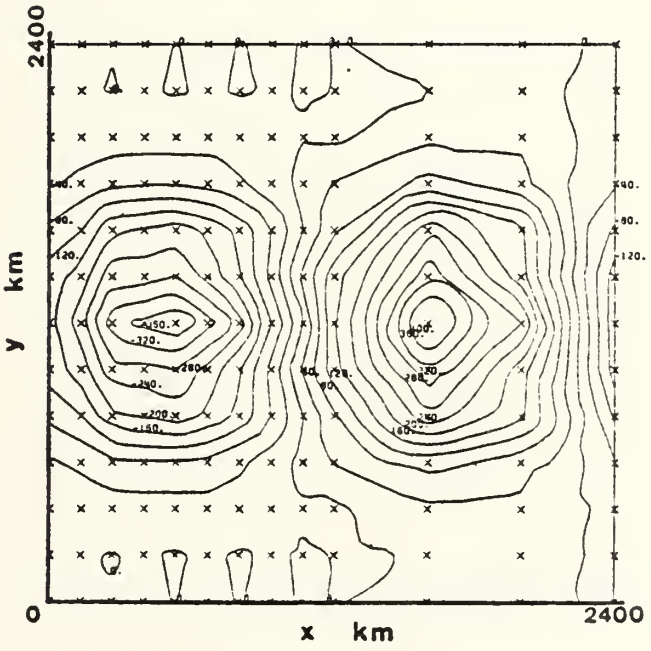

Figure 33. 48 hour forecast for field in figure 30.

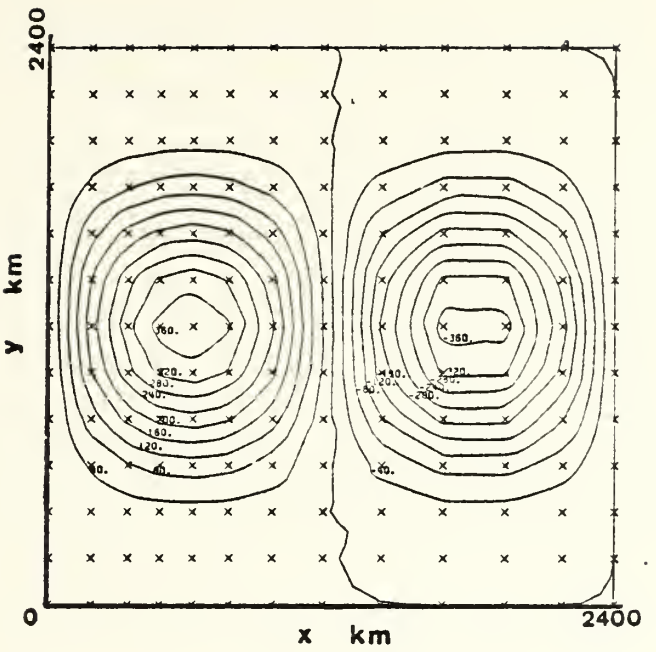

Figure 34. Initial S field with smooth change of resolution (Case 9).

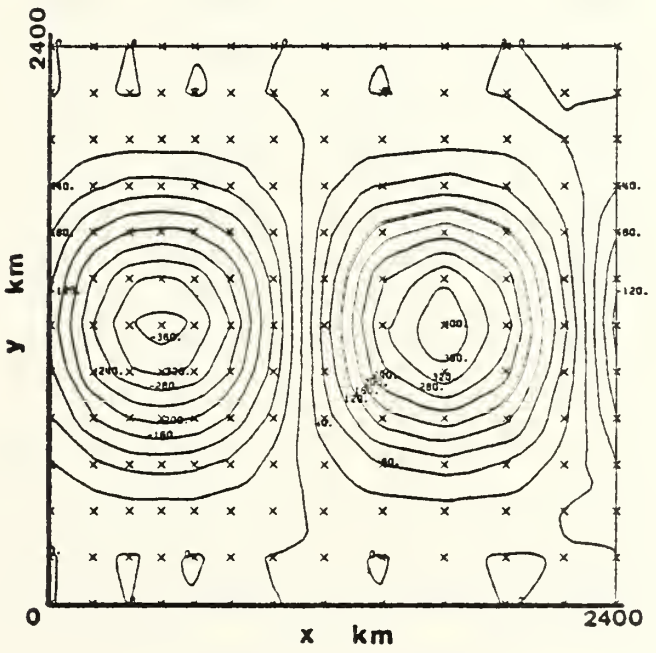

Figure 35. 48 hour forecast for field in figure 34.

of 42 runs are made to study the effects of wind and the forcing term. The 42 runs are formed into 14 tests in which the wind ratios are specified as 0.0 for uniform flow and 0.2 and 0.4 for variable flow. The tests include cases that have both uniform and non-uniform resolution, both equilateral and right triangular elements and the 13 x 12 and 13 x 24 nodal arrangements. Table III contains the results of 12 of the runs which comprise four tests. In 12 of the total of 14 tests, the model performs better with the uniform wind. In all tests once the wind is non-uniform the forecasts are degraded as non-uniformity increases.

TABLE III

RESULTS OF VARIABLE WIND, "FLIPPED" WIND AND FORCING TERM TESTS

		UNFORCED			FORCED		
CASE	RATIO	RMSE	SPEED	CORR.	RMSE	SPEED	CORR.
			NORMAL				
13	0.0	2.9	1.004	.9996	2.9	1.004	.9996
14	0.2	3.4	1.005	.9995	3.3	1.005	.9995
15	0.4	8.7	1.006	.9970	8.7	1.006	.9970
			FLIPPED				
16	0.0	2.8	1.005	.9996	2.8	1.007	.9996
17	0.2	2.7	1.004	.9996	2.6	1.004	.9997
18	0.4	3.1	1.005	.9995	2.9	1.004	.9960

J. "FLIPPED" WINDS

Up until now, the initial conditions, in conjunction with the transformation of coordinates scheme, require that the area of highest wind is also the area of highest resolution, provided, of course, that both the wind and the resolution are non-uniform. Now, downstream of the area of highest winds is an area of convergence and downstream of the area

of lowest wind is an area of divergence. Therefore, where the convergence runs into the divergence is the area where the gradients are highest. It is a "bottleneck". But that is exactly the area where the resolution is the most coarse. The forecast should improve if the grid or initial wind pattern could be "flipped" to concentrate the nodes in the area of minimum winds. Since "flipping" the grid requires fewer changes, that is the choice here. As an example, Figures 36 and 37 are the initial field and 48 hour forecast of such an arrangement.

To verify this reasoning, 24 runs are formed into 12 tests. Cases 13, 14, and 15 on Table III are "normal" whereas Cases 16, 17 and 18 are "flipped". In all tests, the "flipped" arrangement yields superior forecasts. This result justifies the reasoning that the high resolution should be concentrated in area of highest gradients, not the areas of fastest flow.

K. FORCING TERM

The forcing term was developed in Chapter VIII as an alternate method of testing the forecast if the general form of the end product is known. The 42 runs form 21 pairs of forced/unforced tests, some of which are in Table III. The forced forecasts are slightly better in 15 tests, the unforced are slightly better in five tests. One test comes out a tie. In general, the unforced forecasts are better if the wind is uniform while a non-uniform wind favors the forced forecast. However, all differences are very slight. Figures 38 and 39 are the initial field and 48 hour forecast respectively for a typical forced forecast with a uniform wind. They should be compared with Figures 28 and 29 which form the corresponding unforced case.

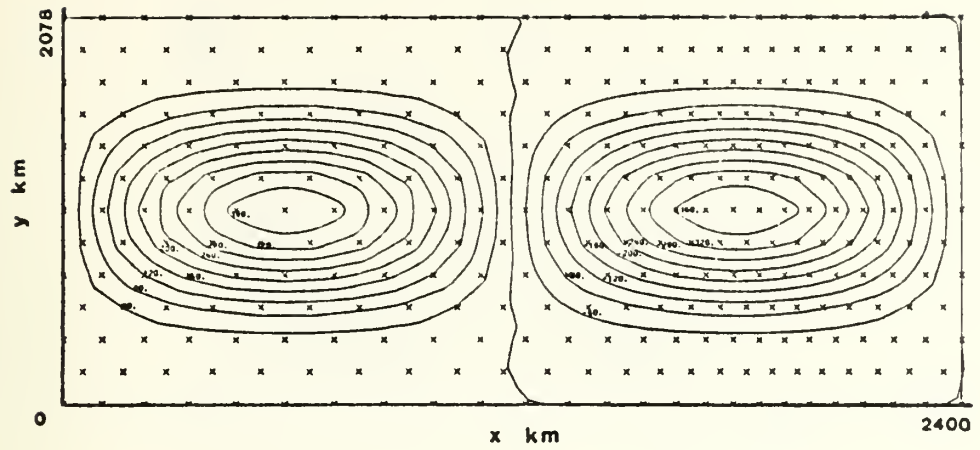

Figure 36. Initial S field with "flipped" winds. $r_1 = 2$, $r_2 = 1$ and R = 0.2.

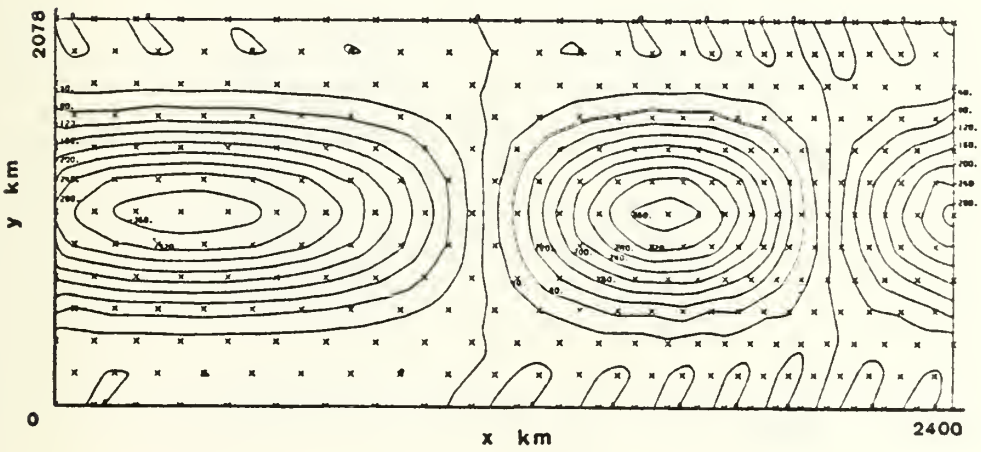

Figure 37. 48 hour forecast for field in figure 36.

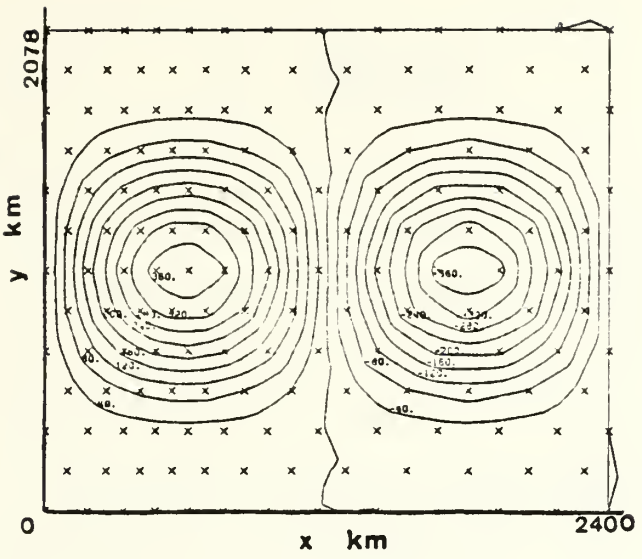

Figure 38. Initial S field for a typical forced case.

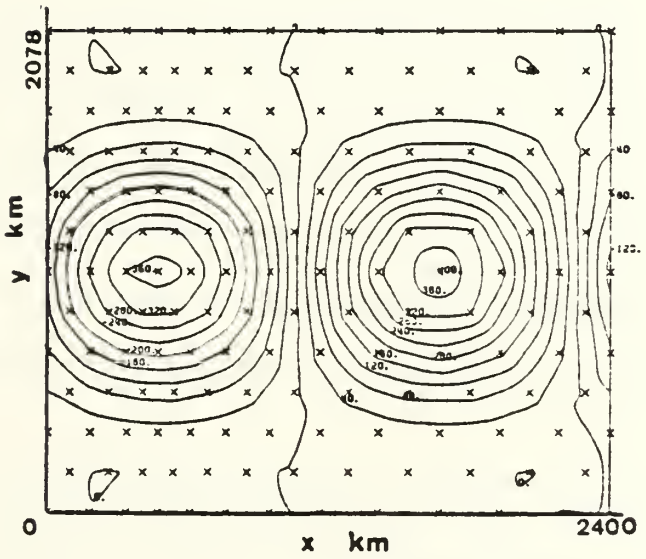

Figure 39. 48 hour forecast for field in figure 38.

XI. CONCLUSIONS

This report applies the Finite Element Method to the two-dimensional advection equation with diffusion. Although the underlying equation is simple enough, FEM models have certain inherent advantages, which include very accurate phase speeds and the ability to change resolution easily. However, they also have limitations, such as a relatively high computational cost, and a requirement for fairly sophisticated and efficient programming. The purpose of this investigation is to establish some guidelines and provide qualitative methods that may be used in the development of future FEM models.

The conclusions are given below in the same order as they are discussed in Chapter X:

1. The model yields reasonable and consistent results. There appear to be no major algorithmic or coding problems as all the results are mathematically and meteorologically plausible.
2. Diffusion is an effective noise filter; however it does have a maximum usable limit which must be independently determined for each application. Numerical models should contain at least some provision for diffusion.
3. The Robert filter is also a valuable feature to have built into a model. In general, the filter should be no heavier than absolutely needed to control high frequency noise. This model uses a filter of 0.1; higher values are not recommended.

4. The model handles wave numbers 1 and 2 well (24 and 12 nodes per wave, respectively) and wave number 3 (8 nodes per wave) with less accuracy. Higher wave numbers maintain accurate phase speeds although RMSE deteriorates.
5. Formulations with elements as equilateral triangles outperform those with elements as right triangles. The difference in RMSE is about 20 percent. The right triangle formulation generates spurious short waves which may be be the primary cause of the relative inaccuracy.
6. Adding nodes (and hence, elements) to the domain will improve the model if they are added symmetrically. More nodes allow smoother transition between fine and coarse resolution. This smoothness is critical.
7. An unexpected result is that this model performs better when the resolution is varied with the flow rather than across it. The reasons for this are unclear.
8. The most important conclusion of this investigation is that the smoother and slower the change in the resolution, the better the forecast. In this model the smooth change reduces the RMSE by 62 percent over the abrupt change.
9. The model works best with uniform flow. In general, as the flow departs from uniformity, the forecast continues to degrade.
10. The forecast can be improved by concentrating the high resolution areas in the region of the strongest gradients.
11. Inclusion of a term that forces the supposed solution back into the model may yield slightly better forecasts. It forms a valid, alternative method to test numerical models.

LIST OF REFERENCES

Bathe, K., and Wilson, E. L., 1976: Numerical Methods in Finite Element Analysis. Prentice-Hall, 528 pp.

Crandall, S. H., 1956: Engineering Analysis. McGraw-Hill, 417 pp.

Cullen, M. J. P., 1973: A Simple Finite Element Method for Meteorological Problems. J. Inst. Maths. Applics., v. 11, 15-31.

Haltiner, G. J., and Williams, R. T., 1980: Numerical Prediction and Dynamic Meteorology, 2d Ed. Wiley, 477 pp.

Kelly, R. G., and Williams, R. T., 1976: A Finite Element Prediction Model with Variable Element Sizes. Naval Postgraduate School Report NPS-63Wu 76101, 103 pp.

Robert, A. J., 1966: The Integration of a Low Order Spectral Form of the Primitive Meteorological Equations. J. Meteor. Soc. Japan, v. 44, 237-245.

Staniforth, A. N., and Daley, R. W., 1977: A Finite-Element Formulation for the Vertical Discretization of Sigma-Coordinate Primitive Equation Models. Mon. Wea. Rev., v. 105, 154-169.

_____, and Mitchell, H. L., 1978: A Variable-Resolution Finite-Element Technique for Regional Forecasting with the Primitive Equations. Mon. Wea. Rev., v. 106, 439-447.

INITIAL DISTRIBUTION LIST

		No. Copies
1.	Defense Technical Information Center Cameron Station Alexandria, Virginia 22314	2
2.	Library, Code 0142 Naval Postgraduate School Monterey, California 93940	2
3.	Dr. R. T. Williams, Code 63Wu Department of Meteorology Naval Postgraduate School Monterey, California 93940	8
4.	Chairman, Code 68Mr Department of Oceanography Naval Postgraduate School Monterey, California 93940	1
5.	Chairman, Code 63Rd Department of Meteorology Naval Postgraduate School Monterey, California 93940	1
6.	Director Naval Oceanography Division Naval Observatory 34th and Massachusetts Avenue NW Washington, DC 20390	1
7.	Commander Naval Oceanography Command NSTL Station Bay St. Louis, Mississippi 39522	1
8.	Commanding Officer Naval Oceanographic Office NSTL Station Bay St. Louis, Mississippi 39522	1
9.	Commanding Officer Fleet Numerical Oceanography Center Monterey, California 93940	1

10. Commanding Officer — 1
Naval Ocean Research and Development Activity
NSTL Station
Bay St. Louis, Mississippi 39522

11. Commanding Officer — 1
Naval Environmental Prediction Research Facility
Monterey, California 93940

12. Chairman, Oceanography Department — 1
U. S. Naval Academy
Annapolis, Maryland 21402

13. Chief of Naval Research — 1
800 N. Quincy Street
Arlington, Virginia 22217

14. Office of Naval Research (Code 480) — 1
Naval Ocean Research and Development Activity
NSTL Station
Bay St. Louis, Mississippi 39522

15. Program Manager (CIRF) — 1
Air Force Institute of Technology
Wright-Patterson Air Force Base, Ohio 45433

16. Commander — 1
Air Weather Service
Scott Air Force Base, Illinois 62225

17. Commanding Officer — 1
Air Force Global Weather Central
Offutt Air Force Base, Nebraska 68113

18. Capt. M. Older — 5
SD/WE
P. O. Box 92960
Worldway Postal Center
Los Angeles, California 90009

19. Dr. A. Arakawa — 1
Department of Meteorology
University of California
Los Angeles, California 90024

20. Dr. David A. Archer — 1
Douglas DuPont Rachford, Inc.
6150 Chevy Chase
Houston, Texas 77027

21. Dr. M.J.P. Cullen — 1
Meteorological Office
Bracknell Berks, United Kingdom

22. Dr. R. L. Elsberry, Code 63Es — 1
Department of Meteorology
Naval Postgraduate School
Monterey, California 93940

23. Dr. J. A. Galt — 1
NOAA - Pac Mar Envir Lab
University of Washington
Seattle, Washington 98105

24. Prof. G. J. Haltiner, Code 63Ha — 1
Department of Meteorology
Naval Postgraduate School
Monterey, California 93940

25. Dr. R. L. Haney, Code 63Hy — 1
Department of Meteorology
Naval Postgraduate School
Monterey, California 93940

26. Capt. J. Hayes, Code 63 — 1
Department of Meteorology
Naval Postgraduate School
Monterey, California 93940

27. Lcdr D. Hinsman, Code 63 — 1
Department of Meteorology
Naval Postgraduate School
Monterey, California 93940

28. Dr. A. Kasahara — 1
National Center for Atmospheric Research
P. O. Box 3000
Boulder, Colorado 80303

29. Dr. Robert L. Lee — 2
Atmospheric and Geophysical Sciences Division
University of California
P. O. Box 808
Livermore, California 94550

30. Prof. N. A. Philips — 1
National Meteorological Center/NOAA
World Weather Building
Washington, DC 20233

31. Dr. T. Rosmond — 3
Naval Environmental Prediction Research Facility
Monterey, California 93940

32. Prof. D. Salinas, Code 69Zc — 1
Department of Mechanical Engineering
Naval Postgraduate School
Monterey, California 93940

33. Dr. Y. Sasaki — 1
Department of Meteorology
University of Oklahoma
Norman, Oklahoma 73069

34. Dr. Andrew Staniforth — 1
Recherce en Prevision Numerique
West Isle Office Tower, 5 ieme etage
2121 route Trans-Canada
Dorval, Quebec H9P1J3, Canada

35. Dr. W. C. Thacker — 1
National Oceanic and Atmospheric Administration
15 Rickenbacker Causeway
Miami, Florida 33149

36. Prof. C. Wash, Code 63Wy — 1
Department of Meteorology
Naval Postgraduate School
Monterey, California 93940

37. Capt. E. Woodward, Code 37 — 1
Computer Science Curricular Office
Naval Postgraduate School
Monterey, California 93940

38. Prof. O. C. Zienkiewicz — 1
Head of Civil Engineering Department
University of Wales
University College of Swansea
Singleton Park
Swansea SA2 8PP, United Kingdom

Thesis
03695
c.1

193743

Older

A two-dimensional finite element advection model with variable resolution.